NASA CONTRACTOR REPORT

NASA CR-280

PLANETARY METEOROLOGY

by George Ohring, Wen Tang, and Joseph Mariano

Prepared under Contract No. NASw-975 *by*
GCA CORPORATION
Bedford, Mass.
for

NATIONAL AERONAUTICS AND SPACE ADMINISTRATION • WASHINGTON, D. C. • AUGUST 1965

NASA CR-280

PLANETARY METEOROLOGY

By George Ohring, Wen Tang, and Joseph Mariano

Prepared under Contract No. NASw-975 by
GCA CORPORATION
Bedford, Mass.

for

NATIONAL AERONAUTICS AND SPACE ADMINISTRATION

For sale by the Clearinghouse for Federal Scientific and Technical Information
Springfield, Virginia 22151 – Price $3.00

TABLE OF CONTENTS

LIST OF ILLUSTRATIONS

LIST OF ILLUSTRATIONS (continued)

PLANETARY METEOROLOGY

By George Ohring, Wen Tang and Joseph Mariano

SUMMARY

Studies are performed on the meteorology of the planet Mars, Venus, and Jupiter.

Mars

Inferences concerning atmospheric circulation features on Mars are made from analysis and interpretation of some observed Martian cloud systems and from application of meteorological theory to the Martian atmosphere. The trajectories of several cloud systems and the use of two different theoretical criteria suggest the presence of a wave type circulation regime on Mars. Cloud observations also suggest the presence of subtropical high pressure centers, and upper level meridional flow and frontal phenomena at equatorial latitudes. The mean large scale zonal velocity is estimated to be about 25 m/sec. Techniques for estimating maximum surface winds and the percentage frequency of occurrence of high surface winds are discussed. Based upon theoretical computations of the vertical velocity profile and analogy with the earth's atmosphere, the Martian troposphere is estimated to extend to about 20 km.

Venus

Radiative equilibrium temperatures are computed for the surface and atmosphere of Venus. In the model used for the computations, it is assumed that the atmosphere and cloud cover are both grey in the infrared. The solar radiation that is not reflected back to space is assumed to reach the surface of the planet. The effect on the computed surface temperature of different values of infrared emissivity, height, and thickness of the cloud layer, and infrared opacity of the gaseous absorbers, is evaluated. The effective infrared emissivity of the cloud layer — which depends upon the emissivity and thickness of the cloud — is found to be the most important factor governing the surface temperature. If the effective cloud emissivity is about 0.99, the high observed surface temperatures of 600-700^{o}K can be maintained by the greenhouse mechanism, even if the atmospheric infrared opacities are rather modest.

Several different theoretical models are used to study the general circulation of the Venusian atmosphere. The models are of two general types: the first type is based upon hypothetical estimates of the radiation budget; the second type is based upon the observed indications of surface temperature gradient between subsolar and antisolar points. In all models, the effect of

the planet's rotation is assumed negligible. The average wind velocities obtained with these models range from 2-30 m/sec. The model that gives the highest wind velocity is probably not too realistic because of too many simplifying assumptions. If the results of this model are eliminated, the average wind velocities range from 2-8 m/sec; these are lower than the average wind velocities in the earth's atmosphere.

Jupiter

Equations are derived for the computation of the radiative equilibrium temperature profile in the non-grey atmosphere above the Jovian cloud layer.

A general survey is conducted of available observational and theoretical information on circulation phenomena in the Jovian atmosphere.

INTRODUCTION

This Final Report covers research performed during the past year on Planetary Meteorology under NASA Contract No. NASw-975. It marks the conclusion of the third year of NASA support of our research on the meteorology of the planets. The primary goal of this research is to increase knowledge of meteorological conditions and processes in the atmospheres of Mars, Venus, and Jupiter. This goal is accomplished through a synthesis of available observations with appropriate meteorological theory.

Emphasis is placed on the thermal state and circulation regimes in these planetary atmospheres. During the past year, research was conducted on: theoretical models of the general circulation on Mars and Venus; inferences of atmospheric circulation processes on Mars from Martian cloud observations; techniques for estimating the maximum wind near the Martian surface; radiative equilibrium temperatures for the surface and atmosphere of Venus and the Venusian greenhouse effect; a model for determining the vertical distribution of radiative equilibrium temperature above the Jovian cloud deck; and, a summary of available observational and theoretical information on circulation processes in the Jovian atmosphere. These research studies are discussed in the remainder of this report.

METEOROLOGY OF MARS

Atmospheric Circulation of Mars

A technical report under this contract treats in detail the research performed on the atmospheric circulation of Mars: Tang, W., 1965: Some Aspects of the Atmospheric Circulation on Mars, Contract NASw-975, GCA Tech. Rpt. No. 65-4-N. We present here only a summary of this technical report.

Inferences from Cloud Observations - Knowledge of clouds is of great value for understanding the atmosphere in which clouds and cloud systems form, grow, and dissipate. The life history and motions of clouds and cloud systems provides direct information on winds and circulation phenomena. The following inferences about Martian circulation features are deduced from several cloud observations:

(1) Observations indicate a tendency for dust cloud systems to form at low latitudes of the winter hemisphere. These dust clouds may form as a result of tropical cyclonic storms or from the strong winds associated with cold polar outbreaks. They tend to move across the equator into the summer hemisphere and curve toward the east at mid-latitudes, suggesting the presence of Martian sub-tropical high pressure areas similar to those on the earth. This transequatorial drift of cloud systems indicates a meridional flow in the upper part of the Martian equatorial atmosphere [1]*. Similar conditions are observed on earth in the Philippine Islands area during late fall or early winter.

(2) If the observed movements of yellow dust clouds are representative of storm movements on Mars, then the average drift velocity of the cloud systems – about 20-30 km hr^{-1} – is probably less than the speed of the broad current in which the storm is imbedded.

(3) Based on cloud photographs of Kuiper [2], it appears that the general circulation on the planet Mars is in the wave regime, as is the case on earth.

(4) Observations indicate that cloud systems analogous to frontal cloud systems on earth exist on Mars. Thus fronts may be a typical meteorological phenomenon of the Martian atmosphere. These cloud systems can extend to a height of 30 km above the surface [3].

(5) If the height of this frontal type cloud extends to the tropopause, then the Martian tropopause is about twice as high as the tropopause of the earth.

---

*Numbers in [ ] throughout text indicate reference numbers.

Theoretical Studies Concerning the Inferences from Clouds.- The purpose of this study is to apply theoretical models to explain observed phenomena and to utilize recent data to study various problems related to the circulation of the Martian atmosphere. Problems considered include the slope of fronts at low latitudes, the magnitude of the mean zonal wind velocity, the possible maximum surface wind speed in storms, the vertical velocity profile with height, and the estimated height of the tropopause. Each of these problems is considered separately below.

The slope of a front.- The sloping narrow cloud formation above the surface in Figure 1 bears a resemblance to a front. However, the slope of this formation is about 1/5, much steeper than terrestrial fronts which have slopes of 1/50 to 1/100 at middle latitudes. A possible explanation is that Martian fronts occur at low latitudes where the Coriolis force is relatively small as compared to the inertial force. Furthermore, the surface atmospheric density of Mars is about 1/40 of the earth's surface density. Therefore, the density contrast between the cold and warm air masses is thus further reduced and can be neglected in the conventional Margules' frontal formula. By considering these effects, a modified formula for frontal slope is established.

This formula is used for the estimation of the slope of the front. Assuming that the wind velocity normal to the front in the cold air is 40 m sec^{-1}, the velocity gradient is 0.5 m sec^{-1} per 100 km, and the shear between cold and warm air mass is 10 m sec^{-1}, the computed slope of the front is 0.22 and the corresponsing angle between the front and horizontal surface wind is about 12^{o}. This value agrees quite well with the observed slope of 0.20 indicated in Figure 1.

It appears from this analysis that the observed cloud systems represent Martian frontal phenomena. In addition, regarding the nature of the cloud, the observed cloud was dull-grey in color and dissipated in late morning, which suggests an ice crystal composition. This lends further credence to possible frontal phenomena on Mars.

The circulation regime. - In order to understand the behavior of the general circulation, one has to determine whether the large scale atmospheric motion is geostrophic and what the general circulation regime is. The criterion used to fulfill these purposes in our work is mainly based upon the thermal Rossby number. If the thermal Rossby number is much smaller than 1 and comparable with that of earth's atmosphere, the large scale atmospheric motion is in geostrophic balance. The numerical value of the thermal Rossby number for the Martian atmosphere is 0.073, which suggests that the Martian atmosphere is in geostrophic balance.

From the thermal Rossby number and the Froude number of a rotating fluid, we can also determine whether the circulation is in a symmetrical or wave regime. This concept was first introduced in Fultz's rotating annulus experiment. Since his experiment is dynamically similar to the atmosphere of a thermally dirven rotating planet, the criterion can apply to the

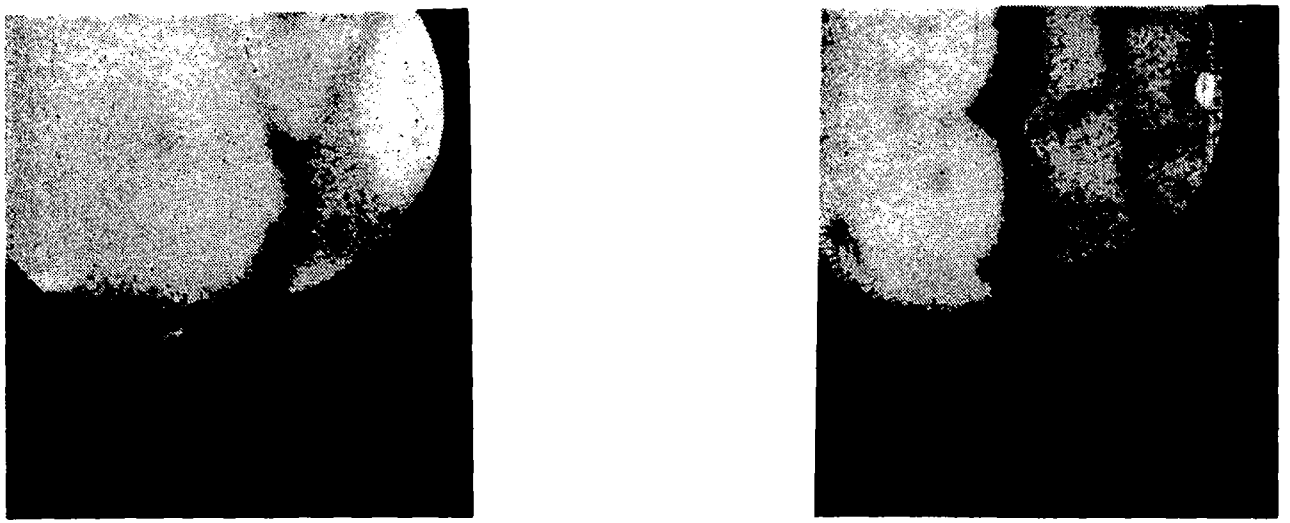

Figure 1. Observations of clouds on the terminator [3]. Case 1. This dull-grey cloud extended over more than 40 degrees in longitude and remained visible for 3 hours with top at about 27 km. Case 2. The dark yellow cloud, which appeared separated from the surface, remained tilted like a frontal cloud, and extended to a height of at least 30 km [3].

atmosphere of Mars. Based on physical parameters of Mars, the Froude number is about 4.3×10^{-3}. If the transition curve for different wave numbers is used, based on Fultz's results, the Martian atmosphere is in a wave regime in the yearly mean.

From consideration of thermal equilibrium, Mintz [4] derived a different criterion for stability of a symmetrical regime. His criterion depends mainly on the total poleward heat transport, which is linearly proportional to the kinematic coefficient of vertical viscosity at the middle level of the atmosphere in his model. If, for Mars, an average coefficient of viscosity is assumed that is the same as the earth's, namely 100 g sec^{-1} cm^{-1}, the conclusion is reached that the general circulation on Mars is in a wave regime in the annual mean, which is in agreement with our conclusion based on the thermal Rossby number and the Froude number.

Mean zonal and meridional wind velocities. - The circulation model of Haurwitz [5] is used to compute the mean zonal and meridional wind velocities on Mars. His model describes the thermally driven, large scale circulations for a rotating planet. In his formula, we need to know the difference of the rate of change of temperature between the equator and pole, the coefficient of friction, the depth of the circulation system, and the Coriolis parameter. Based on the most recent available annual radiation budgets for Mars [4,6] and an appropriate value of coefficient of viscosity, $1/2 \times 10^{-5}$ sec^{-1}, and assuming other parameters the same as on earth, we obtain a zonal velocity between 23 to 30 m sec^{-1} for a surface pressure of 25 mb, and 13 to 16 m sec^{-1} for a surface pressure of 85 mb. The corresponding meridional velocity is 1.5 to 0.6 m sec^{-1}, about 1/20 of the above values.

That the computed average wind speeds on Mars are higher than those computed for earth may be attributed to: (1) a larger difference in the radiational temperature change between equator and pole on Mars then on earth, and (2) a smaller dissipation of kinetic energy by friction on Mars than on earth. Both of these circumstances are an indirect result of a lower Martian surface pressure.

Estimation of the maximum surface wind on Mars. - It is believed that the maximum surface wind on Mars would take place in a strongly rotating vortex. Therefore, a formula for the maximum surface wind velocity for a convective vortex, such as a tropical storm, was used. The important parameter is the central pressure of the vortex, which has to be estimated. If we assume a central pressure 3 mb lower than the environment, the maximum surface wind speed is approximately 140m sec^{-1}. Observations of yellow clouds that extend to heights of 10 km and higher are suggestive of deep convective storms. Pressure drops of 1 to 3 mb in these storms may be possible.

Large scale vertical motion and vertical extent of clouds. - Since the large scale motion on Mars is generally quasi-geostrophic and since the atmosphere may be quasi-static, we can obtain an Omega equation to determine the vertical velocity from a set of vorticity and thermal equations. With the assumption that mean wind velocity decreases linearly with pressure, we obtain a computed profile of vertical velocity as shown in Figure 2. The

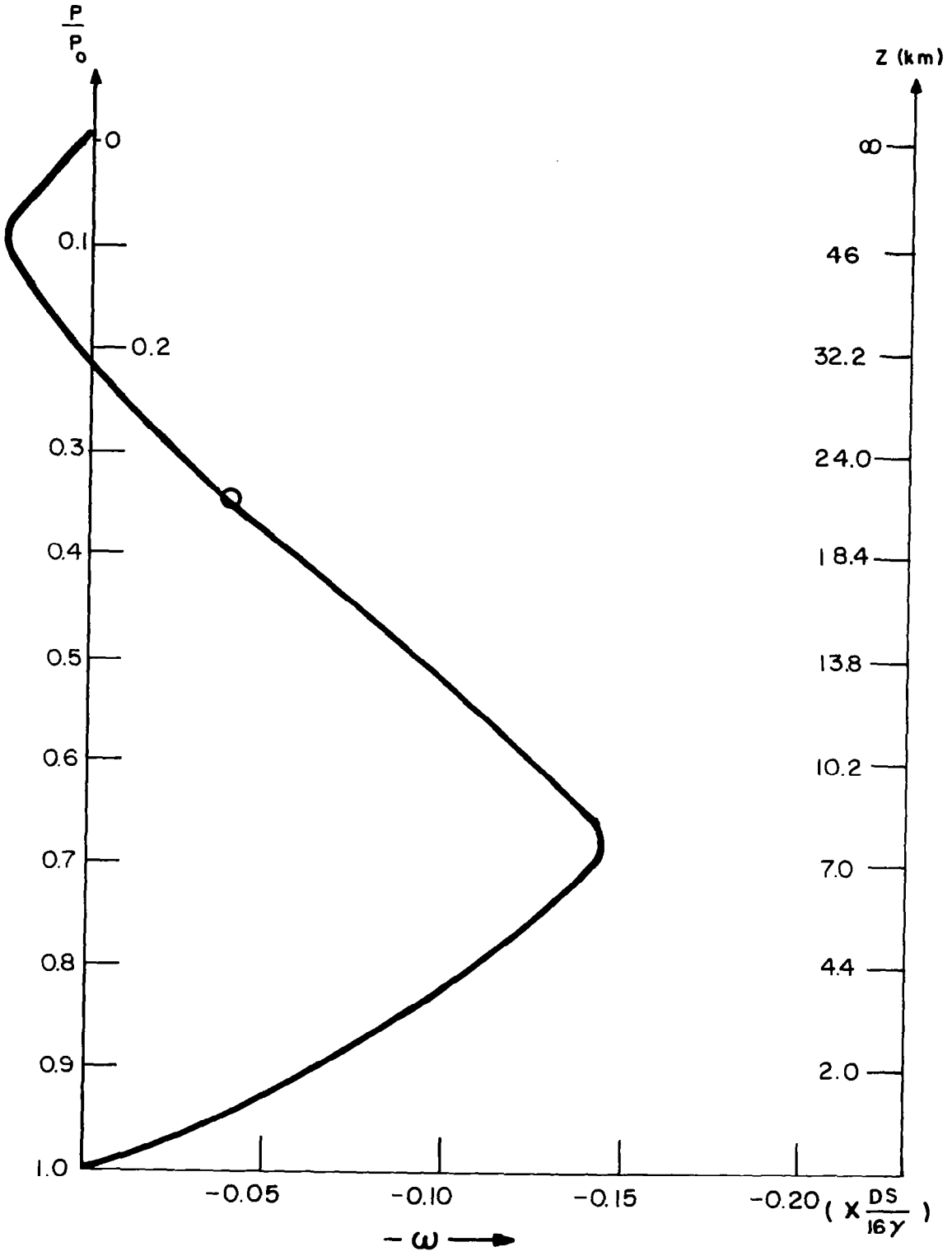

Figure 2. Computed vertical velocity profile for Martian atmosphere ($u_o = v_o = 60$ m sec^{-1}; L = 4000 km; $|S| = 90$ m^2 mb^{-1} sec^{-1} deg^{-1}).

maximum vertical velocity is about 12.8 cm sec^{-1}, which is about four to six times larger than that observed on earth. The determination of the mean tropopause is based on the position of the point of inflection of this profile. From Figure 2 the average tropopause at middle latitudes on Mars is about 20 km.

Design Winds for Martian Landers

A landing vehicle descending through the Martian atmosphere will be subject to horizontal transport by the prevailing atmospheric winds. If there are surface relief features on the planet, such a horizontal transport may lead to possible damage of the vehicle as it is carried horizontally to a collision with the solid surface. To properly design for such a possibility, it is desirable to have an estimate of the maximum wind likely to be encountered near the surface. Although our study of some aspects of the atmospheric circulation on Mars indicates how an estimate of the maximum surface wind can be derived, there is no indication of what percentage of the time such winds may occur. For design purposes, it is usually desirable to have an estimate of the frequency of occurrence of high winds. The following discussion indicates how such estimates may be obtained.

Recently, Ryan [7] and Gifford [8] have presented theoretical estimates of the minimum wind speeds necessary to initiate dust storms in the Martian atmosphere. The yellow clouds in the Martian atmosphere are generally believed to be manifestations of such dust storms. The minimum velocities obtained by these authors for a height of one meter above the surface are listed in Table 1.

TABLE 1

MINIMUM HORIZONTAL WIND SPEED AT A HEIGHT OF 1 METER NECESSARY TO INITIATE DUST STORMS (KM HR^{-1})

	Ryan [7]					Gifford [8]		
	Surface Model 1		Surface Model 2					
k(cm)	80 mb	25 mb	80 mb	25 mb	k(cm)	100 mb	25 mb	10 mb
0.03	40	95	60	145	0.3	14	47	72
0.006	--	--	70	180	---	--	--	--
0.003	--	--	75	190	---	--	--	--

In Table 1, k is a measure of the surface roughness, the pressures refer to the surface pressure on Mars, and Ryan's Models 1 and 2 refer to different

assumptions about the Martian surface. The variation in speeds between Ryan's Surface Model 1 and Gifford's model is mainly due to the difference in assumed surface roughness. A value of k = 0.03 corresponds to the surface roughness of a terrestrial desert. Ryan's Surface Model 2 considers the Martian surface as very smooth, covered with fine grained material, and having a surface roughness less than that of terrestrial deserts. These conditions lead to higher required minimum velocities to initiate grain movement. Regardless of the variation in wind speed among the different models, the important thing is that these authors have developed a model for estimating the threshold wind speeds near the surface that are required to initiate dust storms. If we assume that whenever such a wind speed occurs on Mars, a dust storm and yellow cloud will result, then, by determining the frequency of occurrence of yellow clouds, we can estimate the frequency of occurrence of the threshold wind speeds.

Yellow clouds are known to be a rare occurrence on Mars. However, until recently no one has ever given a quantitative estimate of frequency of occurrence. Recently, Gifford [8] estimated that yellow clouds displaying motion occur slightly more than once per opposition period. This estimate was based upon a search of the literature, and files and publications of various observatories. Over a period of 87 years, only 53 examples of yellow cloud motion could be found. Let us assume that a reasonable estimate of the occurence of yellow clouds is once per opposition period. To be conservative, let us further assume that observations of Mars are only made during a two-month period around opposition, and that all the reported observations of yellow clouds occurred during these two-month periods. This assumption leads to an estimate of one yellow cloud every 60 days. If we assume that the average yellow cloud lasts 1 day and that the wind speeds necessary to initiate the cloud last just as long, we can estimate that threshold wind speeds occur 1/60 of the time. But this assumes that when a threshold wind speeds occurs any place on the planet, a dust storm will result. Actually, one would expect such storms to be initiated only over the "desert like" areas, which cover about 2/3 of the planet. Thus, we should multiply our observed frequency by 3/2, which gives us a probability of occurrence of threshold wind speeds of about 3/120, or about 3%. This means that about 97% of the time the wind speeds near the surface are less than the threshold value. For a surface pressure of 25 mb, the theoretical threshold wind speeds range from about 50 km/hr to 200 km/hr, depending on surface roughness and grain size.

What wind speeds do the yellow cloud drifts reveal? Gifford [8] has tabulated wind speeds derived from all available observations of yellow cloud occurrences. He has divided these occurrences into two classes: (1) yellow clouds, which occur within meters of the surface, and (2) projection clouds, which occur higher in the atmosphere. The average speed of the yellow clouds, based upon fifteen occurrences, is about 29 km/hr; the average speed of the projection clouds, based upon twenty occurrences, is about 70 km/hr. The increase of average speed with height is in qualitative agreement with what one would expect from theory. However, the theoretical threshold wind speeds of 50 km/hr to 200 km/hr for the 25 mb case are not in agreement with the observed

average surface wind speed of 29 km/hr. As discussed by Ryan [7] the most likely explanation for this discrepancy is the probability that the observed cloud drift speeds do not represent wind speeds but rather storm drifts, which are generally less than the wind speeds within the storm. Also, the average wind speed determined from the cloud drifts may not be representative of the threshold speeds that are required to initiate the cloud. The other possibilities are higher surface roughness on Mars or higher surface pressures, both of which seem rather unlikely at the moment.

Thus, although wind speeds derived from observed cloud drifts are not in agreement with the theoretical threshold wind speeds, the concept of using the threshold wind speeds to obtain estimates of the probability of occurrence of maximum winds on Mars still appears to be valid. However, if it is true that the threshold wind speeds are present only at the time of initiation of the dust clouds, our percentage probabilities of occurrence of maximum winds should be lowered since we assumed that they prevailed for an average duration of 1 day, corresponding to the average duration of an individual dust cloud. On the other hand, our estimate of frequency of occurrence of dust clouds may be too low, since dust systems whose size is less than the resolving power of earth based telescopes — $\sim$ 100 km — escape detection. These two factors may compensate each other. For practical utilization of this concept for estimating design winds, improved estimates of the surface roughness and grain size are required, since present uncertainties in these parameters lead to a factor difference of 4 in the estimated threshold wind speeds.

METEOROLOGY OF VENUS

Radiative Equilibrium Temperatures for the Surface and Atmosphere of Venus

Introduction. — Observations of the microwave radiation emitted by Venus have been conducted from earth-based radio astronomy observatories and from the Mariner spacecraft fly-by of the planet. These observations indicate that the surface temperature of Venus is remarkably high — about 600 to 700°K (see for example, References 9 and 10). Such temperatures are two to three times the temperature expected on Venus on the basis of its distance from the sun and its planetary albedo. This discrepancy between the expected and observed surface temperatures has stimulated research on the cause of the high observed surface temperatures.

A strong greenhouse effect as an explanation for the high surface temperature was proposed by Sagan [11]. For the greenhouse mechanism to be effective, the atmosphere must be relatively transparent to incoming solar radiation and relatively opaque to outgoing infrared radiation. On the earth, for example, of the solar radiation that is not reflected back to space, about 75 per cent reaches the surface and is absorbed there [12]. Of the infrared radiation emitted by the surface, only about four per cent is transmitted directly through the atmosphere to space, the remainder being absorbed by water vapor, carbon dioxide, ozone, and clouds in the atmosphere and reradiated back to the surface and to space [12]. The net result of this differential between atmospheric transmissivity or opacity for solar radiation and for infrared radiation is a greenhouse effect that is sufficient to raise the average surface temperature of the earth to 288°K — some 36° above the average temperature the earth would have in the absence of any greenhouse effect.

On Mars, a weaker greenhouse effect is present. Of the solar radiation that is not reflected back to space, about 97 to 98 per cent is transmitted by the atmosphere and absorbed at the surface [13]. However, with small amounts of water vapor, carbon dioxide, and cloudiness, the transmissivity of the atmosphere for infrared radiation is relatively high — about 45 per cent, corresponding to a total infrared opacity of 0.5 [14]. The net result is a greenhouse effect that raises the average surface temperature from 208°K — the temperature Mars would have in the absence of a greenhouse effect, based upon deVaucouleurs' [15] recent estimate of 0.295 for the Martian planetary albedo — to the observed average temperature of about 230°K [16]. Thus, for both earth and Mars, the presence of an atmospheric greenhouse is sufficient to raise the average surface temperature some ten per cent over the values that would prevail if this effect were absent.

As opposed to a greenhouse effect of the order of ten per cent for Mars and earth, the required greenhouse effect on Venus is of the order of 200 to 300 per cent, since the observed surface temperature is 600 to 700°K while the

equilibrium temperature in the absence of a greenhouse effect is only about 237°K. Thus, it is quite obvious that, if the high Venusian surface temperatures are caused by the greenhouse mechanism, the Venusian atmosphere must have a differential between its transmissivity for solar radiation and its transmissivity for infrared radiation that is much greater than that in the atmospheres of Mars and earth. The crux of the matter probably lies in the infrared opacity of the atmosphere, since for any given amount of solar radiation — no matter how small — the surface temperature can be increased to any desired value if the infrared opacity is sufficiently large. The early greenhouse models of the Venusian atmosphere ascribed the large required infrared opacity solely to the gaseous constituents of the Venusian atmosphere. However, Jastrow and Rasool [17] pointed out that such large infrared opacities were incompatible with present knowledge of the amounts of infrared absorbing gases in the atmosphere. Öhring and Mariano [18] suggested that the clouds in the Venusian atmosphere might play a major role in maintaining an efficient greenhouse effect. The water and ice clouds in the earth's atmosphere contribute to the earth's greenhouse effect by preferentially transmitting solar radiation while absorbing infrared radiation. Observations of Venus do indeed indicate that the planet is covered by a permanent cloud cover, which may be composed of ice [19]. Thus, with about twice as much average cloudiness as on earth, the Venusian greenhouse effect may be substantially enhanced by the presence of clouds. By including the contribution of clouds to the greenhouse effect, Öhring and Mariano [18] showed that, with 99 per cent cloudiness, surface temperatures of 600 to 700°K could be maintained with atmospheric infrared opacities of three to seven (infrared transmissivities of two per cent to 0.02 per cent), respectively. Such atmospheric infrared opacities are more nearly in line with the computed infrared opacity ($\sim$ 5) [20] of the amounts of carbon dioxide and water vapor believed to be present in the Venusian atmosphere. The model used, however, contained several assumptions that can be improved upon. For example, the clouds were assumed to be completely opaque to infrared radiation. Recent observations of infrared radiation [21] in the earth's atmosphere indicate that earthly clouds are, in general, not opaque to infrared radiation. The form of the atmospheric temperature profile used in the model was specified in advance, rather than computed with the model. To eliminate these restrictions, we can develop a radiative equilibrium greenhouse model in which the infrared opacity of the clouds can be varied and the atmospheric temperatures, as well as the surface temperature, can be computed. This model can be used to evaluate the effect of the infrared opacity, height, and thickness of the clouds on the computed surface and atmospheric temperatures on Venus. Such a model and the computations performed with it are discussed in the following sections.

Radiative Equilibrium Model. — It is assumed that the Venusian surface and atmosphere are in radiative equilibrium. The atmosphere is assumed to be gray in the infrared. At some height in the atmosphere, a complete cloud cover is present, which is also assumed to be gray in the infrared with an effective infrared emissivity ϵ_c. Atmospheric and cloud absorption of solar radiation are neglected. The atmospheric infrared opacity is taken as zero at the surface of the planet and increases to the value τ_g at the top of the

atmosphere. In Figure 3, the physical model is shown schematically. The requirements for radiative equilibrium can be stated as: (1) the atmosphere above and below the cloud layer is in infrared radiative equilibrium, and (2) the upward infrared radiation flux at the top of the atmosphere is equal to the net incoming solar radiation.

The net flux of infrared radiation at any level τ above the cloud top can be written as

$$F(\tau) = 2\epsilon_e E_3(\tau-\tau_c) + 2\int_{\tau_c}^{\tau} B(t)E_2(\tau-t)dt + [2B_o E_3(\tau_b) + 2\int_{o}^{\tau_b} B(t)E_2(\tau_b-t)dt] \cdot$$

$$(1-\epsilon_e)2E_3(\tau-\tau_c) - 2\int_{\tau}^{\tau_g} B(t)E_2(t-\tau)dt \qquad (1)$$

where F is the net flux of infrared radiation; ϵ_e is the effective emissivity of the cloud layer; τ is atmospheric infrared opacity; B is the black body flux, equal to σT^4, where σ is the Stefan-Boltzmann constant, and T is temperature; the E's are exponential integrals; and the subscripts o, b, c, and g refer to the surface, the cloud base, the cloud top, and the top of the atmosphere, respectively. The first two terms on the right hand side of Equation (1) represent the contributions to the upward radiation flux at τ from the cloud and from the atmosphere between the cloud top and τ, respectively; the third term represents the contribution to the upward flux at τ from the surface and atmosphere below the cloud base; and the last term represents the downward flux of radiation at τ due to the atmosphere above τ. The effective emissivity of the cloud layer is composed of two parts: a part due to the emissivity of the cloud substance itself and a part due to the infrared absorbing gases in the cloud layer. The infrared transmissivity of the cloud layer in the absence of the cloud is simply $2E_3(\tau_c-\tau_b)$; the transmissivity of the cloud substance in the layer is $(1-\epsilon_c)$. The effective transmissivity of cloud plus atmosphere in the cloud layer is $(1-\epsilon_c)2E_3(\tau_c-\tau_b)$. The effective emissivity of the cloud layer is simply one minus the effective transmissivity, or

$$\epsilon_e = 1 - [(1-\epsilon_c)2E_3(\tau_c-\tau_b)] \quad . \qquad (2)$$

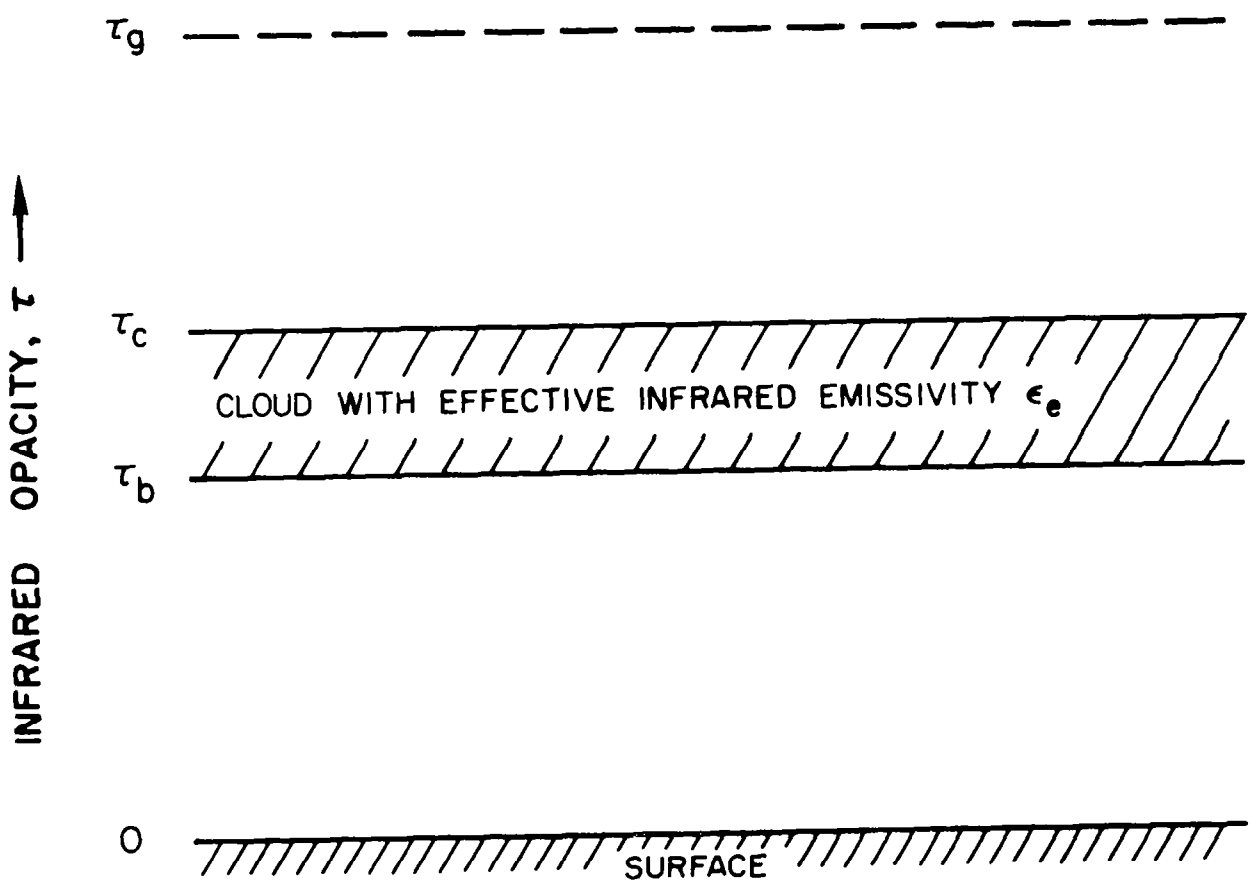

Figure 3. Schematic diagram of physical model used in radiative equilibrium temperature calculations.

The net flux of infrared radiation at any level below the cloud base can be written in a similar fashion as

$$F(\tau) = 2B_o E_3(\tau) - 2\epsilon_e B_b E_3(\tau_b-\tau) + 2\int_o^{\tau} B(t)E_2(\tau-t)dt - 2\int_{\tau}^{\tau_b} B(t)E_2(t-\tau)dt -$$

$$- [2\int_{\tau_c}^{\tau_g} B(t)E_2(t-\tau_c)dt](1-\epsilon_e)2E_3(\tau_b-\tau) \quad . \tag{3}$$

Applying the radiative equilibrium condition for the atmosphere,

$$\frac{dF}{d\tau} = 0 \ , \tag{4}$$

we obtain the following relationships:

Above the cloud

$$2B(\tau) = \epsilon_e B_c E_2(\tau-\tau_c) + \int_{\tau_c}^{\tau_g} B(t)E_1(|\tau-t|)dt + 2[B_o E_3(\tau_b) +$$

$$+ \int_o^{\tau_b} B(t)E_2(\tau_b-t)dt](1-\epsilon_e)\ E_2(\tau-\tau_c) \quad . \tag{5}$$

Below the cloud

$$2B(\tau) = B_o E_2(\tau) + B_b \epsilon_e E_2(\tau_b-\tau) + \int_o^{\tau_b} B(t)E_1(|\tau-t|)dt +$$

$$+ 2[\int_{\tau_c}^{\tau_g} B(t)E_2(t-\tau_c)dt](1-\epsilon_e)E_2(\tau_b-\tau) \quad . \tag{6}$$

From the condition that the upward infrared radiation flux at the top of the atmosphere must balance the net incoming solar radiation, we obtain

$$2\epsilon_e B_c E_3(\tau_g-\tau_c) + 2\int_{\tau_c}^{\tau_g} B(t)E_2(\tau_g-t)dt + [2B_o E_3(\tau_b) + 2\int_{o}^{\tau_b} B(t)E_2(\tau_b-t)dt] \cdot$$

$$(1-\epsilon_e)2E_3(\tau_g-\tau_c) = \sigma T_e^4 \qquad (7)$$

where T_e is the effective temperature of the net incoming solar radiation.

If we assume that the cloud top and cloud base have temperatures equal to the temperatures of the atmospheric layers immediately adjacent to them, we can solve the numerical analogues of Equations (5), (6), and (7) for the surface temperature and for the vertical distribution of temperature in the atmosphere above and below the cloud. The necessary input parameters are ϵ_e, T_e, τ_g, τ_c, and τ_b.

Numerical Techniques. — By dividing the atmosphere into m layers of equal infrared opacity, τ_b/m, below the cloud, and n layers of equal infrared opacity, $(\tau_g-\tau_c)/n$, above the cloud, as shown in Figure 4, the integral Equations (5), (6), and (7), can be transformed into a system of n+m+1 simultaneous, linear equations for the unknown quantities, $X_1 = T_1^4$, $X_2 = T_2^4$, ..., $X_m = T_m^4$, the fourth power of the temperature at the mid-point of each of the m layers below the cloud; $X_{m+1} = T_{m+1}^4$, $X_{m+2} = T_{m+2}^4$, ..., $X_{m+n} = T_{m+n}^4$, the fourth power of the temperature at the mid-point of each of the n layers above the cloud; and $X_{m+n+1} = T_o^4$, the fourth power of the temperature at the ground. In matrix form, these simultaneous equations are represented by the equation,

$$\begin{pmatrix} & & \\ & A_{ij} & \\ & & \end{pmatrix} \begin{pmatrix} X_1 \\ X_2 \\ \cdot \\ \cdot \\ \cdot \\ X_{n+m+1} \end{pmatrix} = \begin{pmatrix} B_1 \\ B_2 \\ \cdot \\ \cdot \\ \cdot \\ B_{m+n+1} \end{pmatrix} \qquad (8)$$

where the elements of the matrices (A_{ij}) and (B_i) are calculated from Equations (5), (6), and (7) in the following manner.

Equation (5) is applied at the mid-point of each layer above the cloud ($i = m+1, m+2, \ldots, m+n$), producing n equations of the unknown quantity, $X_j = T_j^4$, $j = m+1, m+2, \ldots, m+n$. For the $j^{\underline{th}}$ layer above the cloud the integrals in Equation (5) become (see Figure 4):

$$\int_{\tau_c}^{\tau_g} T^4(t) E_1(|\tau_{m+j+\frac{1}{2}} - t|)\,dt = \sum_{k=m+1}^{m+j-1} \int_{\tau_k}^{\tau_{k+1}} X_k E_1(\tau_{m+j+\frac{1}{2}} - t)\,dt + \tag{9}$$

$$+ 2\int_{\tau_{m+j}}^{\tau_{m+j+\frac{1}{2}}} X_j E_1(\tau_{m+j+\frac{1}{2}} - t)\,dt + \sum_{k=m+j+1}^{m+n} \int_{\tau_k}^{\tau_{k+1}} X_k E_1(t - \tau_{m+j+\frac{1}{2}})\,dt,$$

and,

$$\int_{o}^{\tau_b} T^4(t) E_2(\tau_b - t)\,dt = \sum_{k=1}^{m} \int_{\tau_{k-1}}^{\tau_k} X_k E_2(\tau_m - t)\,dt\ , \tag{10}$$

where the subscripted τ's are the infrared opacities shown in Figure 4, X_k is the fourth power of the temperature at the middle of the $k^{\underline{th}}$ layer, $k = m+1, m+2, \ldots, m+n$, and the E's are exponential integrals. It is assumed that the temperature is constant within each layer. Hence the X's can be taken out of the integrals, and Equation (9) and (10) can be integrated analytically to give

$$\int_{\tau_c}^{\tau_b} T^4(t) E_1(|\tau_{m+j+\frac{1}{2}} - t|)\,dt = \sum_{k=m+1}^{m+j-1} X_k[E_2(\tau_{m+j+\frac{1}{2}} - \tau_{k+1}) - E_2(\tau_{m+j+\frac{1}{2}} - \tau_k)] +$$

$$+ 2X_j[E_2(o) - E_2(\tau_{m+j+\frac{1}{2}} - \tau_{m+j})] + \tag{11}$$

$$+ \sum_{k=m+j+1}^{m+n} X_k[E_2(\tau_k - \tau_{m+j+\frac{1}{2}}) - E_2(\tau_{k+1} - \tau_{m+j+\frac{1}{2}})]\ ,$$

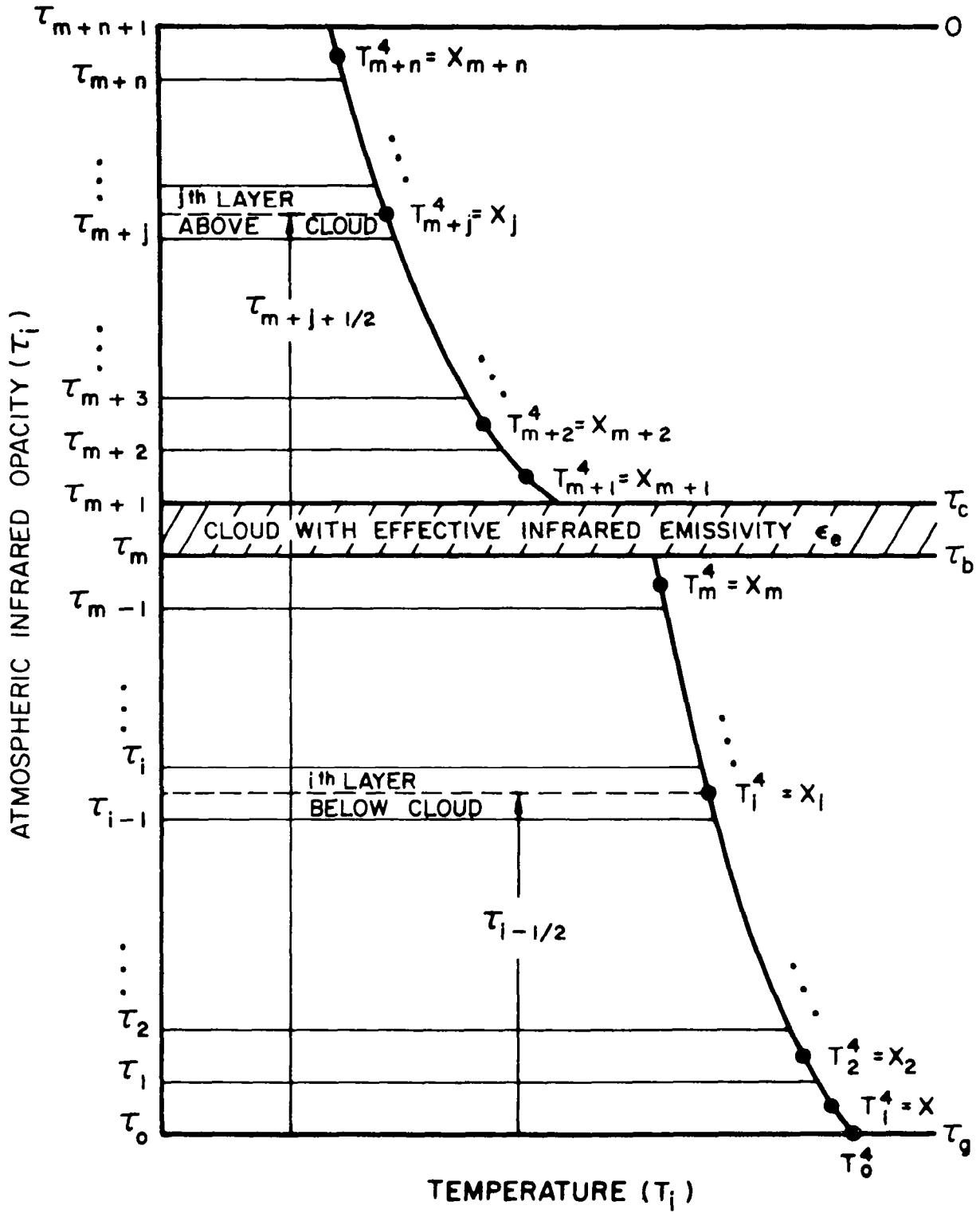

Figure 4. Division of atmosphere into layers for numberical calculations.

and,

$$\int_{o}^{\tau_b} T^4(t)E_2(\tau_b - t)dt = \sum_{k=1}^{m} X_k[E_3(\tau_m - \tau_k) - E_3(\tau_m - \tau_{k-1})] \quad . \qquad (12)$$

Equation (6) is applied at the mid-point of each of the m layers below the cloud, and Equation (7) is applied at the top of the atmosphere, producing the remaining m+1 equations.

By the same method as above, the remaining integrals of Equation (6) and (7) become:

$$\int_{o}^{\tau_b} T^4(t)E_1(|\tau_{i-\frac{1}{2}} - t|) = \sum_{k=1}^{i-1} X_k[E_2(\tau_{i-\frac{1}{2}} - \tau_k) - E_2(\tau_{i-\frac{1}{2}} - \tau_{k-1})] + 2X_i[E_2(o) - E_2(\tau_{i-\frac{1}{2}} - \tau_{i-1})] +$$

$$+ \sum_{k=i+1}^{m} X_k[E_2(\tau_{k-1} - \tau_{i-\frac{1}{2}}) - E_2(\tau_k - \tau_{i-\frac{1}{2}})] \quad , \qquad (13)$$

and,

$$\int_{\tau_c}^{\tau_g} T^4(t)E_2(t - \tau_c) = \sum_{k=m+1}^{m+n} X_k[E_3(\tau_k - \tau_{m+1}) - E_3(\tau_{k+1} - \tau_{m+1})] \quad . \qquad (14)$$

The final assumption is that the temperatures at the upper and lower boundaries of the cloud are equal to the temperatures at the mid-points of the adjacent upper and lower layers, respectively,

$$T(\tau_c) = T_{m+1} \quad ,$$

$$T(\tau_b) = T_m \quad . \qquad (15)$$

Then, by replacing the integrals, $T(\tau_c)$, $T(\tau_b)$, and T_o with Equations (11) to (15), Equations (5) to (7) reduce to the required set of linear, simultaneous Equation (8). A computer program which computes and solves Equation (8) for the radiative equilibrium temperatures T_1, T_2, ..., T_{m+n}, and T_o, for a maximum of fourteen layers, (m+n+1 = 15), has been constructed. In this program the E's are calculated by methods explained in detail by Ohring and Mariano[13].

Results. — Since most of the parameters required for use with the model are ill defined at present, a series of calculations was performed to evaluate the effect on the computed temperatures of changes in the input parameters. The total infrared opacity of the atmospheric gases is uncertain, but Plass and Stull's [20] study suggests that a range of 3 to 7 for τ_g might cover the degree of uncertainty. Calculations are performed with τ_g = 3, 5, and 7. The infrared opacity of the atmosphere above the cloud top was estimated from the ratio of cloud top pressure to surface pressure, since in a grey atmosphere the opacity is proportional to atmospheric pressure. Estimates of the cloud top pressure range from 0.1 to 1 atm [22]. The surface pressure might be in the range 7.5 to 75 atm. The minimum ratio of cloud top pressure to surface pressure is then 0.1/75, or 1.33×10^{-3}; the maximum ratio is 1/7.5, or 1.33×10^{-1}. With a given total atmospheric infrared opacity, the infrared opacity of the atmosphere above the cloud top can be determined from these ratios. The thickness of the cloud layer is also unknown. Computations were performed for a range of $(\tau_c - \tau_b)$ from 0 to 1.0. On the basis of terrestrial analogy and the 8 to 12μ infrared observations of the planet, the cloud emissivity is probably greater than 0.9. Most of the computations were performed using cloud emissivities between 0.9 and 0.99. The only parameter that was not varied is T_e, the effective temperature of the net incoming solar radiation. With a planetary albedo of 0.73 [23], T_e is 237°K.

Since we would like to estimate the enhancement of the greenhouse effect due to the presence of clouds, we first compute the radiative equilibrium temperature distribution in the absence of any clouds. With the use of the Eddington approximation, the following formulas for the atmospheric and surface temperatures, respectively, can be derived:

$$T^4(\tau) = T_e^4\left(\frac{1}{2} + \frac{3\tau}{4}\right) ,$$

$$T_o^4(\tau_g) = T_e^4\left(1 + \frac{3\tau_g}{4}\right) .$$

In these formulas, τ is taken as 0 at the top of the atmosphere and increases downwards to the value τ_g at the surface. Temperature profiles for τ_g = 3, 5, and 7 are shown in Figure 5. (The logarithmic τ scale is approximately equivalent to a linear height scale.) The computed surface temperatures range from 318°K to 377°K, obviously much lower than the observed surface temperatures of 600-700°K. An increase in the total atmospheric infrared opacity from 3 to 7 raises the surface temperatures some 60°K.

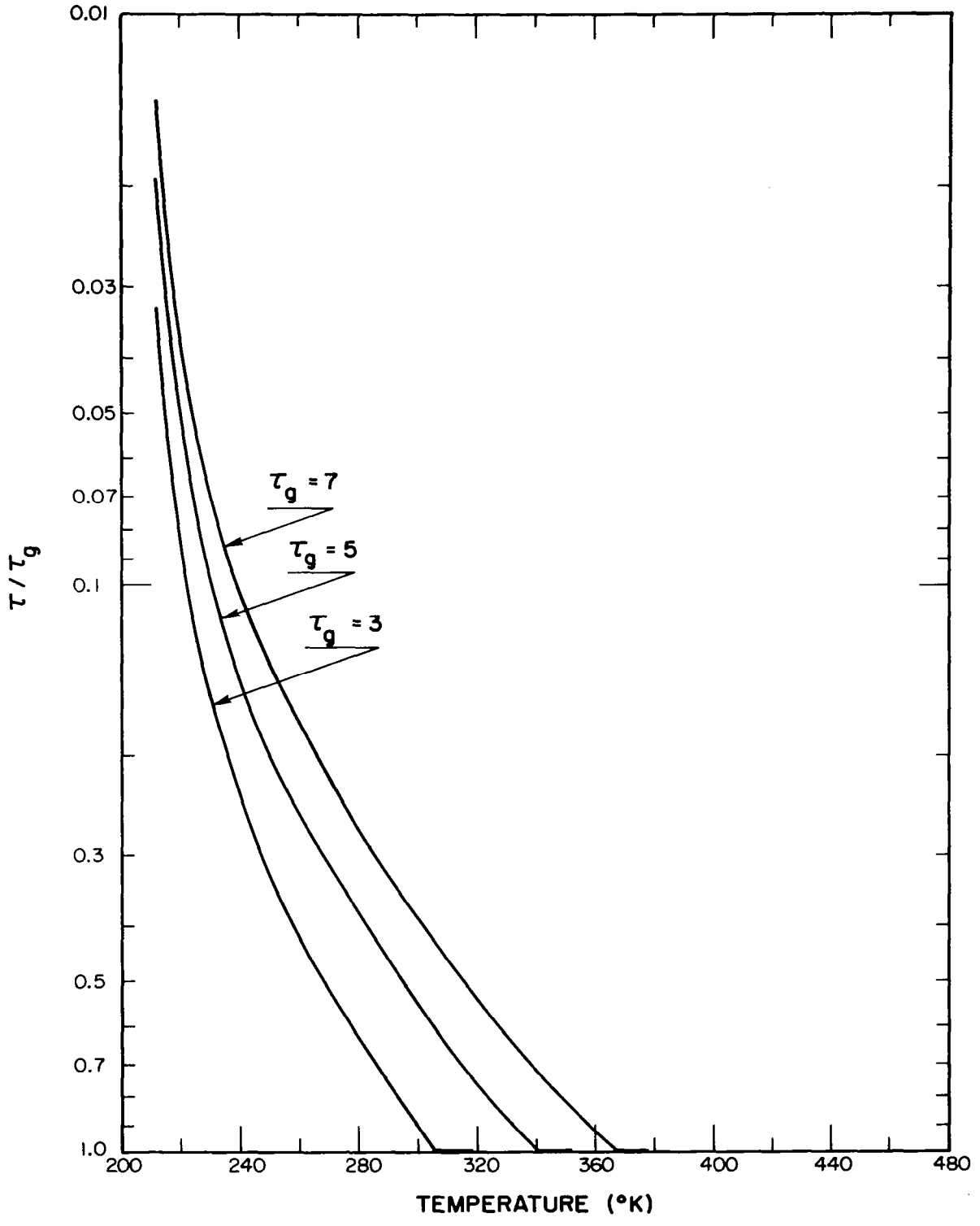

Figure 5. Radiative equilibrium temperature profiles for clear skies computed with Eddington approximation (τ_g = 3, 5, and 7).

To check our computational model against the Eddington approximation, we perform a calculation with an infinitesimal, transparent cloud $\{\epsilon = 0; (\tau_c - \tau_b) = 0\}$ located at some level in the atmosphere. In Figure 6, the results of this computation, performed for $\tau_g = 7$, are compared with the corresponding Eddington approximation calculation. The agreement between the profiles is excellent, suggesting that our model and numerical procedures are sufficiently accurate for this type of computation.

The effect of introducing a cloud into the atmosphere is shown in Figure 7. Here, temperature profiles are shown for $\tau_g = 5$, $\tau_c/\tau_g = 1.33 \times 10^{-2}$, and for cloud emissivities, ϵ_c, equal to 0 (corresponding to clear sky case), 0.5, 0.9, 0.95, and 0.99. (In the remainder of the paper, τ will be taken as zero at the top of the atmosphere and will increase downwards.) The cloud is assumed to have no thickness in these calculations so that the effective cloud emissivity, ϵ_e, is equal to ϵ_c. The computed surface temperature varies from 351°K for clear skies to 637°K for a cloud with an emissivity of 0.99, with most of the change taking place when the cloud emissivity is greater than 0.95. As the cloud emissivity increases, the temperatures below the cloud increase and approach a more nearly isothermal state. The temperatures above the cloud, on the other hand, remain constant. As the cloud emissivity increases, the cloud transmissivity decreases. Thus, less of the surface and sub-cloud atmospheric radiation is transmitted through the cloud. But this is compensated for by higher radiation intensities due to the higher temperatures below the cloud. The net result is an upward flux of radiation at the cloud top that does not depend upon cloud emissivity. Hence, the temperatures above the cloud do not vary with changing cloud emissivity. It is to be noted that as the cloud emissivity increases, the temperature difference between the cloud base and top increases. In a real atmosphere, such large temperature differences would result in super-adiabatic lapse rates, which would lead to convective readjustment of the vertical temperature profile.

The effect of varying the cloud top height is illustrated in Figure 8, in which radiative equilibrium profiles are shown for $\tau_c/\tau_g = 1.33 \times 10^{-3}$, 1.33×10^{-1}, and 5.00×10^{-1}, all for a total atmospheric infrared opacity of $\tau_g = 7$ and for a cloud with an infrared emissivity of 0.99 and no thickness. The computed surface temperature is not particularly sensitive to large changes in the cloud top height, varying only between 640°K to 691°K, with the higher temperatures corresponding to the lower clouds. These surface temperatures are in agreement with the observed Venusian surface temperatures. As expected the cloud top temperature increases significantly as the cloud height decreases, since lowering the cloud is equivalent to increasing the infrared opacity of the atmosphere above the cloud. These calculations indicate that the height of the cloud layer does not appreciably affect the greenhouse mechanism on Venus if the atmosphere is in radiative equilibrium. However, for an atmosphere in convective equilibrium, the height of the cloud top significantly affects the magnitude of the greenhouse effect [18], with higher surface temperatures associated with higher cloud tops.

Without clouds, a change in the total atmospheric infrared opacity from 3 to 7 causes a change of some 50°K in the radiative equilibrium surface

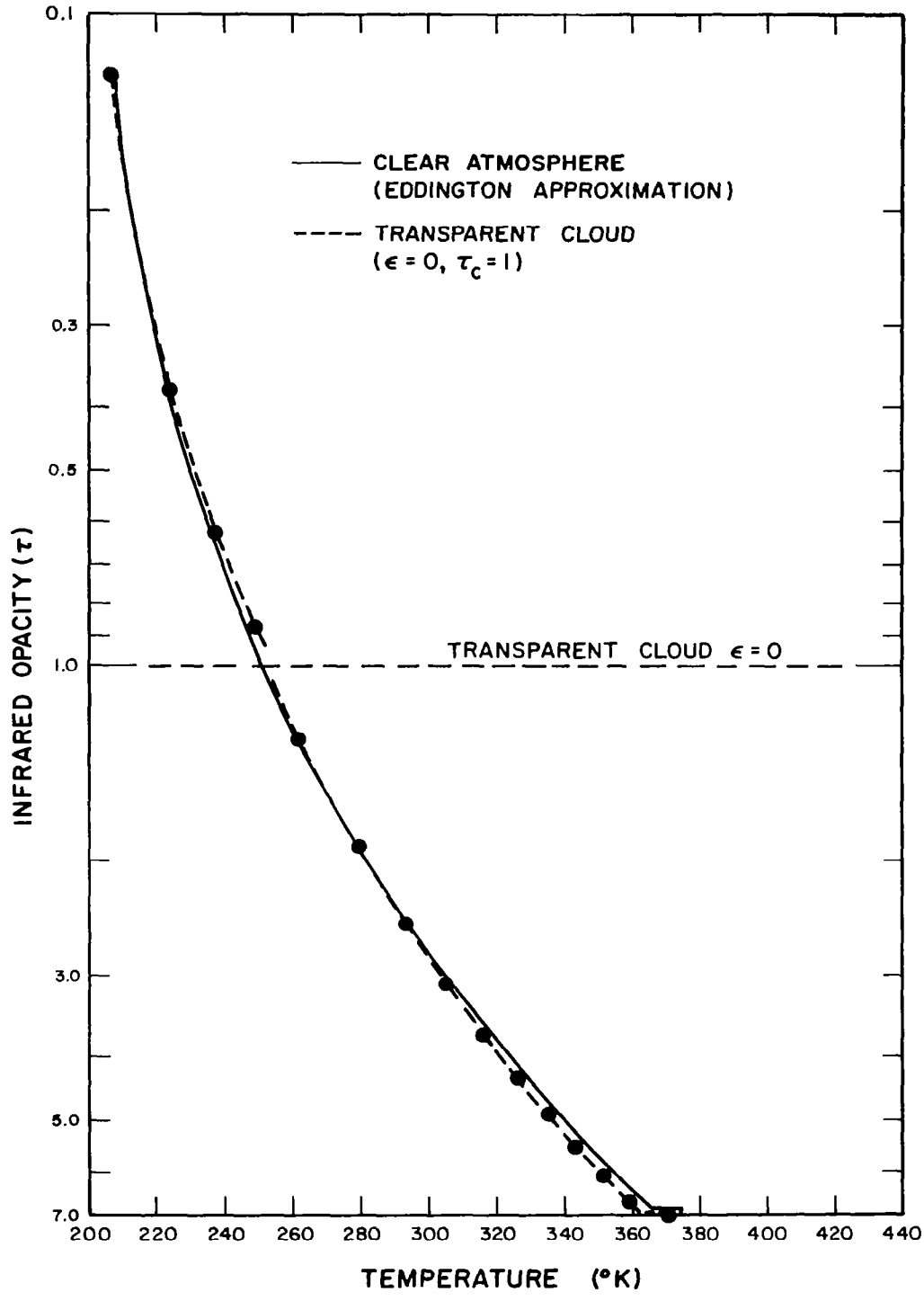

Figure 6. Comparison of Eddington approximation temperature profile for clear skies with temperature profile computed with infinitesimal transparent cloud [$\tau_g = 7$; $\epsilon = 0$; $(\tau_b - \tau_c) = 0$].

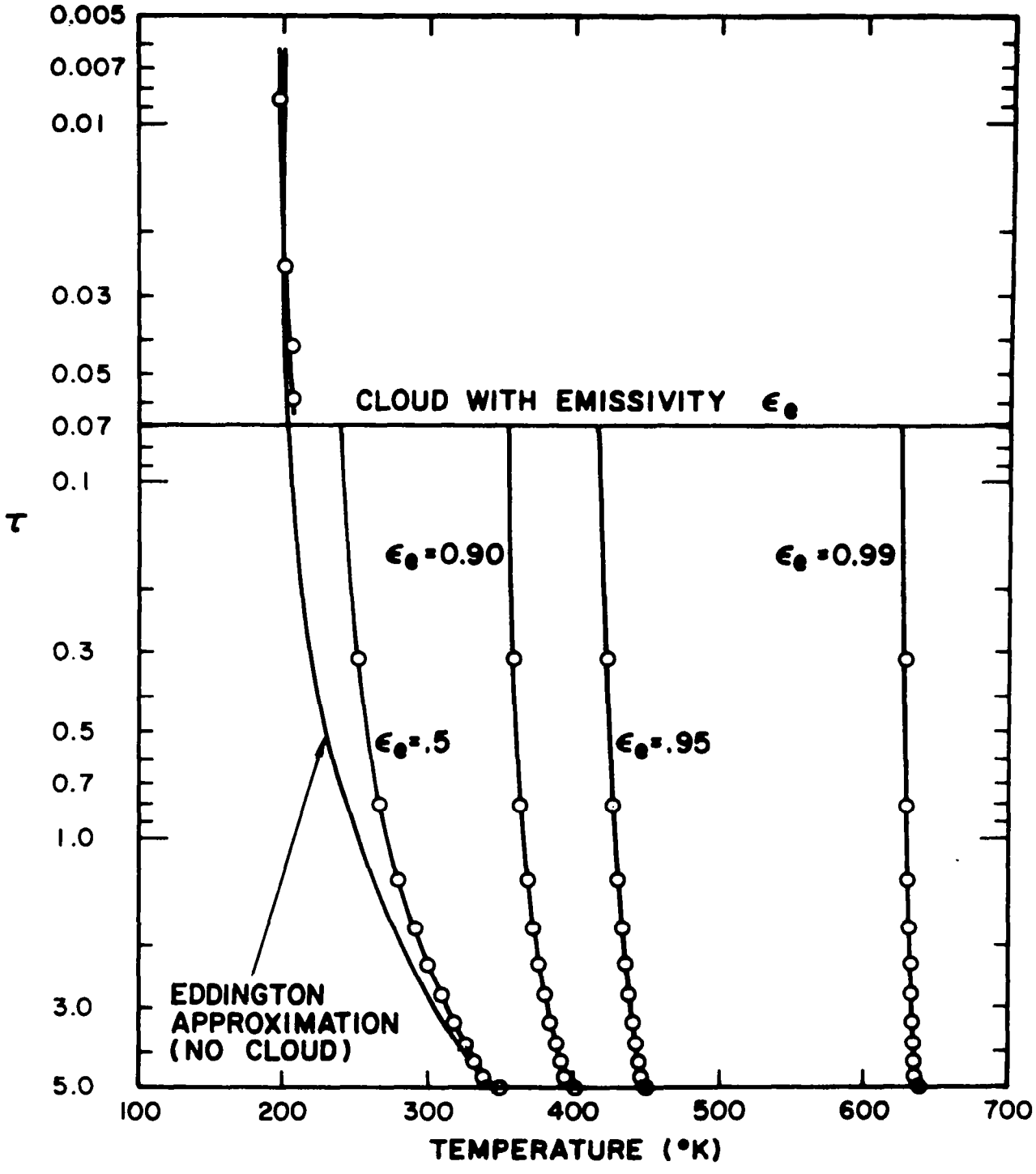

Figure 7. Computed radiative equilibrium temperature profiles for a range of cloud emissivity values (0 to 0.99). Cloud has no thickness $\tau_g = 5$, and $\tau_c/\tau_g = 1.33 \times 10^{-2}$).

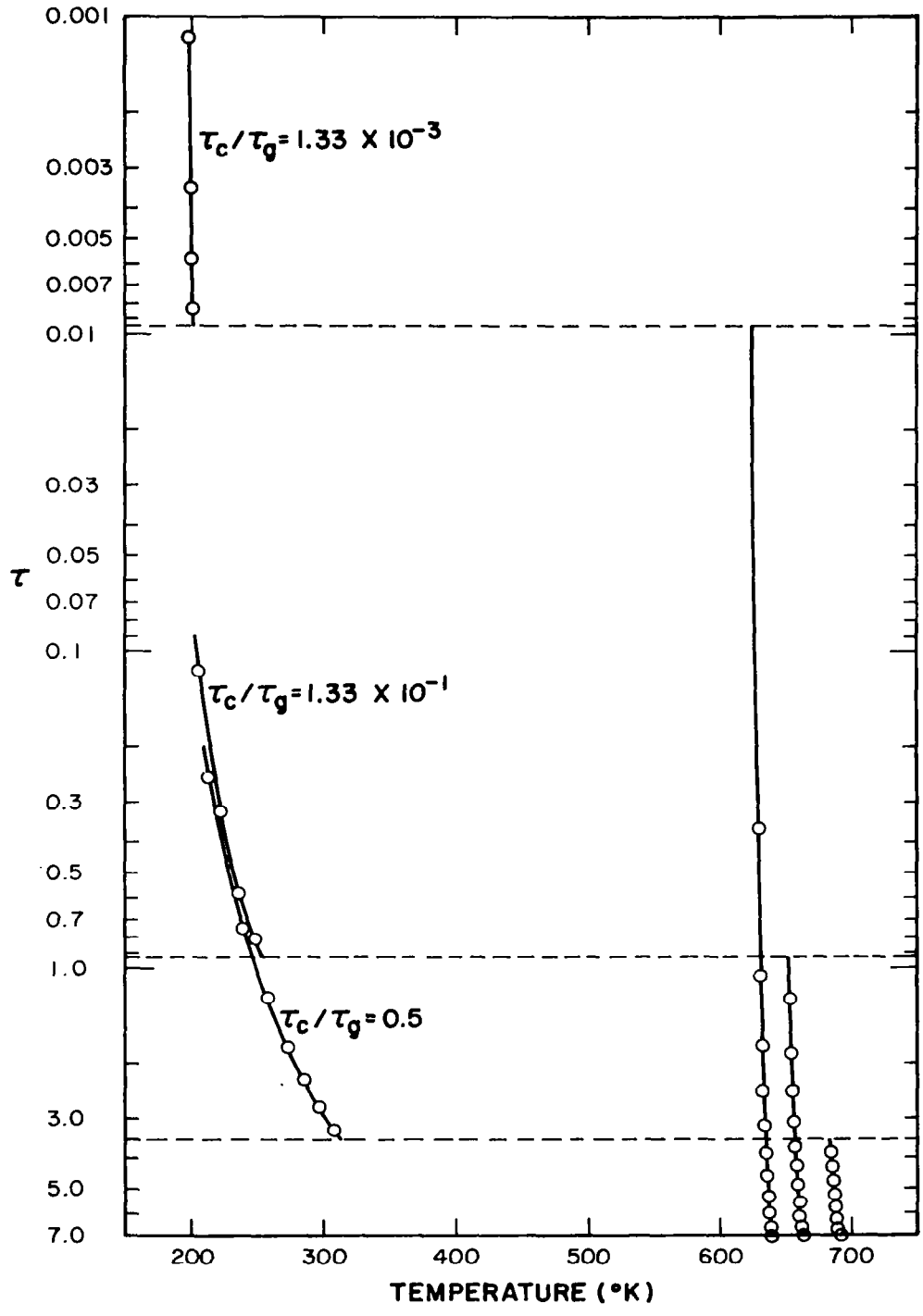

Figure 8. Computed radiative equilibrium temperature profiles for a range of cloud heights (τ_c/τ_g = 1.33 x 10^{-3}, 1.33 x 10^{-1}, and 0.5). Cloud has no thickness, τ_g = 7, ϵ_c = 0.99.

temperature. With clouds, the variation in surface temperature associated with a change of τ_g from 3 to 7 decreases as the emissivity of the clouds increases. For a cloud emissivity of 0.99, the variation is as low as 5°K — from 658°K to 663°K ($\tau_c/\tau_g = 1.33 \times 10^{-1}$). Thus, if the infrared emissivity of the Venusian clouds is high enough, a strong greenhouse effect can be attained, even though the infrared opacity of the atmosphere may be modest.

Thus far, we have discussed infinitesimally thin clouds. As the cloud thickness increases, the effective emissivity of the cloud layer increases, and one would expect the radiative equilibrium surface temperature to increase also. This is indeed seen to be the case in Figure 9, where computed temperature profiles are shown for three cloud thicknesses — $(\tau_b - \tau_c) = 0$, 0.1, and 1.0 — and for $\tau_g = 5$, $\epsilon_c = 0.95$, and $\tau_c/\tau_g = 1.33 \times 10^{-2}$. These calculations show that even if the cloud emissivity is as low as 0.95, a surface temperature of > 600°K can be produced if the cloud is thick enough — thick enough to attain an effective emissivity of the cloud substance plus absorbing gas within the cloud layer that is ~ 0.99.

The most critical parameter in the determination of the surface temperature is the effective emissivity of the cloud. In Figure 10, all the computed surface temperatures are plotted against $(1-\epsilon_e)$, the effective transmissivity of the cloud layer. The points plotted in Figure 10 are based upon the cases listed in Table 2, from which it can be seen that a wide range of values of infrared opacity of the atmosphere, cloud emissivity, cloud top height, and cloud thickness are included. Despite the variations in these other parameters, the computed surface temperatures fall on a rather smooth curve when plotted against effective transmissivity of the cloud layer, suggesting that this parameter is the crucial one for a large greenhouse effect on Venus. The high observed surface temperatures can be maintained if the effective emissivity of the cloud layer is about 0.99. For a surface temperature of 600°K, an effective emissivity of about 0.985 is required; for 700°K, about 0.993 is required. If these are breaks in the cloud cover, higher effective emissivities would be required.

The computed cloud top temperatures are independent of effective cloud emissivity and depend only on the value of the infrared opacity above the cloud top. Table 3 lists the computed cloud top temperatures. It can be seen that the cloud top temperature varies from 200°K to 350°K as the infrared opacity of the atmosphere above the cloud varies from 0.005 to 6.0. The observed cloud temperatures of about 235°K together with the results of these computations suggest an infrared opacity of about 0.7 above the cloud layer.

Conclusions. — The cloud layer in the Venusian atmosphere is capable of creating a large greenhouse effect on Venus, even if the atmospheric infrared opacity is rather modest. To maintain the high observed surface temperatures of 600-700°K, the cloud layer must have an effective infrared emissivity of about 0.99. If there are breaks in the cloud cover, higher effective emissivities are required. The influence of the atmospheric infrared opacity and height of the cloud layer on the surface temperature are not as important as the effective emissivity of the cloud layer.

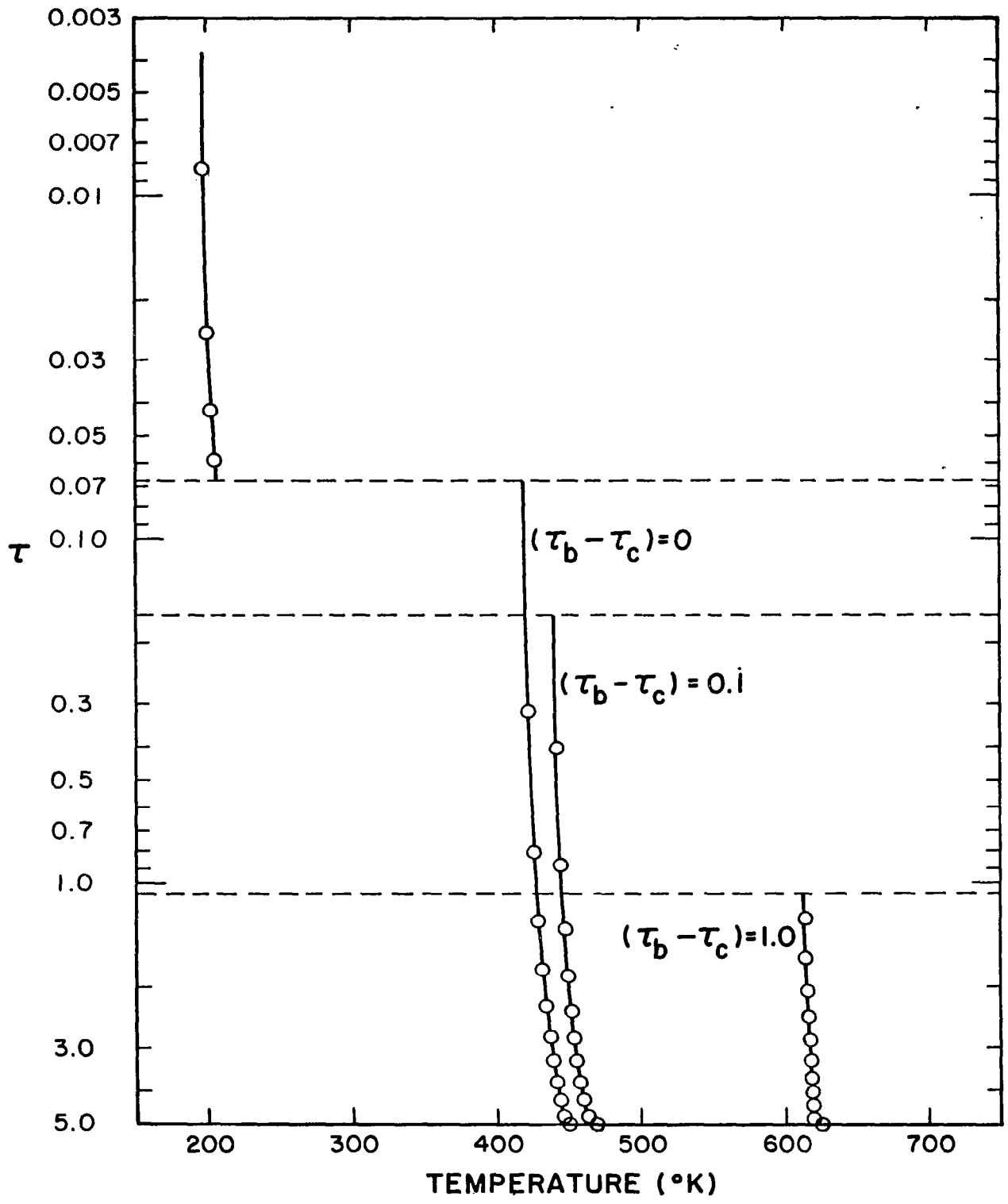

Figure 9. Computed radiative equilibrium temperature profiles for a range of cloud thicknesses [$(\tau_b - \tau_c) = 0$, 0.1, and 1.0)]. $\tau_g = 5$, $\epsilon_c = 0.95$, and $\tau_c/\tau_g = 1.33 \times 10^{-2}$.

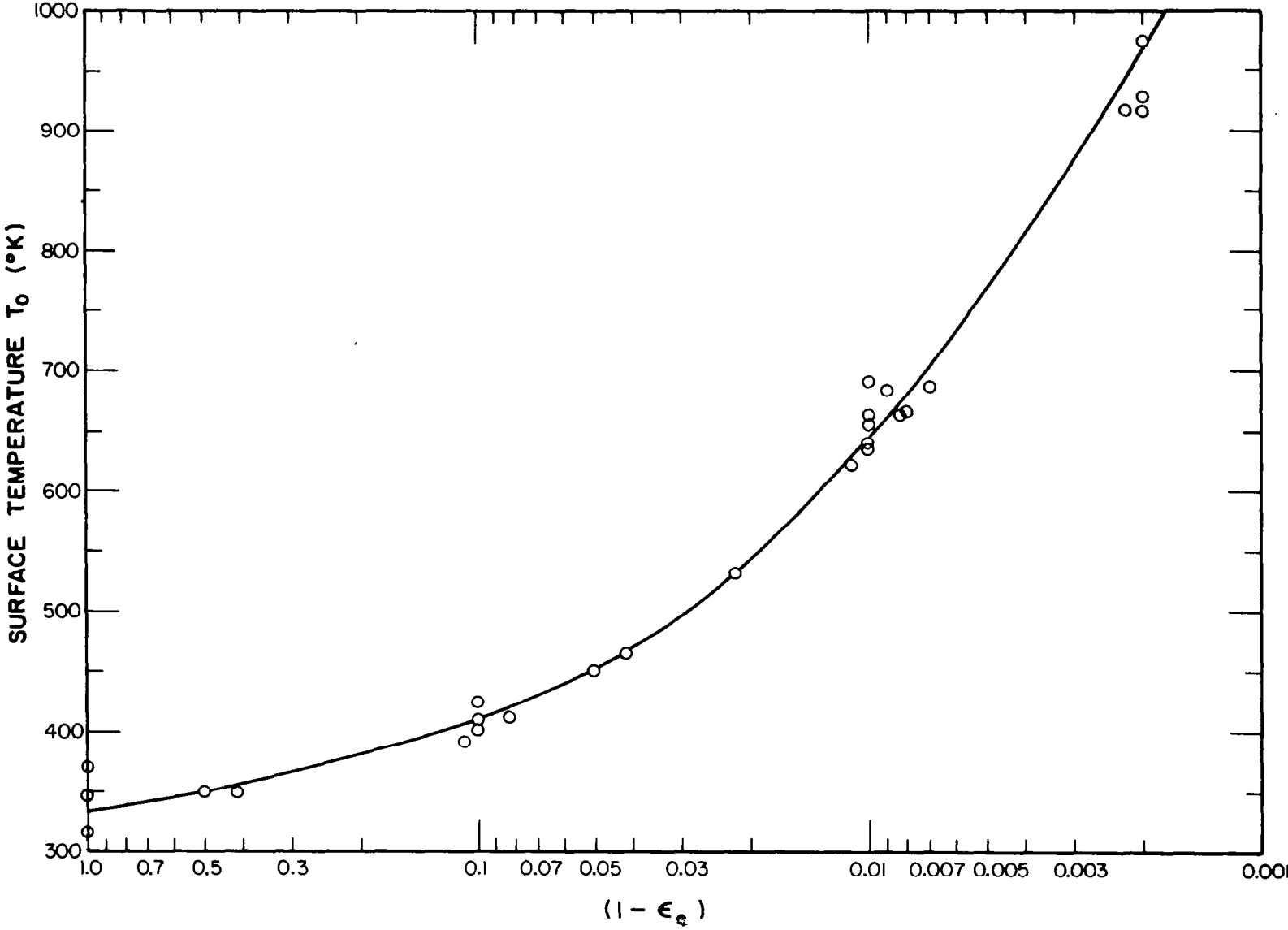

Figure 10. Computed surface temperature as a function of effective transmissivity of cloud layer.

TABLE 2

COMPUTED SURFACE RADIATIVE EQUILIBRIUM TEMPERATURES

τ_g	ϵ_c	$(\tau_b - \tau_c)$	ϵ_e	$1-\epsilon_e$	τ_c/τ_g	T_o (°K)
7	0	0	0	1.0	1.43×10^{-1}	370
7	0	0	0	1.0	8.57×10^{-1}	370
7	0.9	0	0.9	0.1	1.33×10^{-3}	410
7	0.99	0	0.99	0.01	1.33×10^{-3}	640
7	0.9	0	0.9	0.1	1.33×10^{-1}	425
7	0.99	0	0.99	0.01	1.33×10^{-1}	663
7	0.99	0	0.99	0.01	5.00×10^{-1}	691
7	0.99	0.069	0.9912	0.009	1.33×10^{-1}	683
7	0.99	1.069	0.998	0.002	1.33×10^{-1}	977
5	0	0	0	1.0	1.33×10^{-2}	347
5	0.5	0	0.5	0.5	1.33×10^{-2}	349
5	0.9	0	0.9	0.1	1.33×10^{-2}	401
5	0.95	0	0.95	0.05	1.33×10^{-2}	450
5	0.99	0	0.99	0.01	1.33×10^{-2}	637
5	0.5	0.1	0.5837	0.4163	1.33×10^{-2}	350
5	0.9	0.1	0.9169	0.0831	1.33×10^{-2}	412
5	0.95	0.1	0.9584	0.0416	1.33×10^{-2}	466
5	0.99	0.1	0.9917	0.0083	1.33×10^{-2}	666
5	0.5	1.0	0.8903	0.1097	1.33×10^{-2}	391
5	0.9	1.0	0.9781	0.0219	1.33×10^{-2}	531
5	0.95	1.0	0.9890	0.0110	1.33×10^{-2}	622
5	0.99	1.0	0.9978	0.0022	1.33×10^{-2}	919
3	0.99	0	0.99	0.01	1.33×10^{-1}	658
3	0.99	0.1	0.992	0.008	1.33×10^{-1}	688
3	0.99	1.0	0.998	0.002	1.33×10^{-1}	930
3	0.99	0	0.99	0.01	1.33×10^{-2}	638
3	0.99	0.1	0.992	0.008	1.33×10^{-2}	667
3	0.99	1.0	0.998	0.002	1.33×10^{-2}	919

TABLE 3

COMPUTED RADIATIVE EQUILIBRIUM TEMPERATURES OF CLOUD TOP

Infrared Opacity of Atmosphere Above Cloud	Temperature of Cloud Top (^{o}K)
0.005	200
0.009	201
0.040	203
0.066	206
0.399	222
0.931	246
1.000	249
6.000	,50

The computed radiative equilibrium temperature profiles are characterized by a sharp and large temperature decrease from the cloud base to the cloud top. Such a large temperature decrease would lead to super-adiabatic lapse rates in the cloud layer, which would cause convective mixing and a readjustment of the computed temperature profile.

The computed radiative equilibrium cloud top temperatures are independent of effective cloud emissivity and depend only on the infrared opacity of the atmosphere above the cloud. These computations together with the observed cloud temperature of 235°K suggest that the infrared opacity above the cloud is about 0.7.

The General Circulation of Venus' Atmosphere

Introduction. — Recent telescopic measurements of Venus in the microwave region of the spectrum give us quantitative estimates of the planet's surface temperatures and rotation rate. The magnitudes of these quantities have a direct bearing on the required planetary circulation features. This paper presents calculated results of the mean wind velocities and the vertical profile of the wind and temperature fields for Venus' atmosphere, using the radiometric measurements. Several circulation models are used in the calculations, and an intercomparison of their wind velocities is discussed. The reported radial spoke system of cloud patterns on Venus is also explained.

Mean Wind Velocity. — Based on recent evidence, the rotation rate of Venus is about 250 days [24], and, therefore, the Coriolis parameter is about 4×10^{-3} times of that on earth. With such a small rotation rate, it is highly probable that the general circulation is mainly along the meridional direction (here we define the meridional direction in the direction of the lines joining the subsolar and antisolar points, while the zonal direction is in the direction normal to the lines joining subsolar and antisolar points) and that zonal motion is small.

Model of thermally driven circulation by Haurwitz. — Assuming a solar constant of 4.11 cal/cm^2/min and an albedo of 0.75, the effective insolation for Venus is about 1.03 cal/cm^2/min. Assuming that the outgoing radiation is constant all over the planet, we obtain the total difference of heating per unit area between the subsolar and antisolar points, as

$$\Delta[S(1-A)-W] = 1.03 \text{ cal/cm}^2\text{/min} , \qquad (16)$$

where Δ = difference of quantities in the brackets between the subsolar and antisolar point.
S = incident solar radiation (S = solar constant at subsolar point and S = 0 at antisolar point).
A = albedo.
W = outgoing long-wave radiation.

Assuming that the surface pressure is ten atmospheres, that the specific heat at constant pressure for Venus' atmosphere is 0.2 cal/gm/deg and that gravitational acceleration is 880 cm/sec^2, the difference in the rate of temperature change, α, between the subsolar and antisolar points is

$$\alpha = \frac{\Delta[S(1-A)-W]}{c_p \cdot \frac{\Delta p}{g}} = 7.5 \times 10^{-6} \text{ deg/sec} \quad . \tag{17}$$

This quantity serves as an energy source which drives the general circulation of Venus' atmosphere.

Based on Bjerknes' circulation theorem, Haurwitz [5] developed a simple, general model of a thermally driven circulation which includes rotation and frictional dissipation. The mean meridional wind velocity, V, and the zonal velocity, U, at the boundaries of the troposphere approach a steady state condition asymptotically with time, as given by

$$V = \frac{1}{2} \left[\frac{\alpha R \frac{z}{H}}{k(1 + \frac{f^2}{k^2}} \right]^{1/2} \tag{18}$$

and

$$U = \frac{f}{k} V$$

where R = gas constant,

$\frac{z}{H} = \ell n \frac{p_o}{p}$,

p = pressure at top level of the circulation system,

p_o = surface pressure,

k = coefficient of friction,

and f = Coriolis parameter.

Since Venus is considered a synchronously rotating planet, the effect of rotation is negligible, i.e., $f \approx 0$; therefore, the zonal component of wind is zero and the circulation model reduces to a meridional component

$$V = \frac{1}{2} \left[\frac{\alpha R z}{kH} \right]^{1/2} \tag{19}$$

Based on calculations by Kaplan [25], the tropopause is at 0.008 of an atmosphere; thus $\ell n(p_o/p) = 7.14$. Assuming a gas constant of 2.5×10^6 cm^2/sec^2/deg, based on an atmospheric composition of 10% CO_2 and 90% N_2, and a friction coefficient of 5×10^{-5}/sec, five times larger than the value on earth, the steady state meridional wind velocity is 8.12 m/sec.

A coefficient of friction larger than the earth is used since we assume a higher surface pressure (and density) for Venus. The same calculation using the earth's coefficient of friction, $k = 10^{-5}$/sec, yields a higher wind velocity of 18.3 m/sec.

Circulation model for a synchronously rotating planet. — Mintz [26] developed a general model to compute the mean wind velocity for a synchronously rotating planet. He assumes that the energy radiated to space in the dark hemisphere must be replaced by an energy transport across the terminator from the sunlit side. Using a simple two-layer model atmosphere and assuming an equal mass distribution in these two layers, Mintz obtained a formula for the mean wind velocities at the middle levels in each layer. From the equation of continuity, his model demands that the wind speeds in both layers must be equal and opposite in direction, i.e., the mass transport in the upper level must equal the mass transport in the lower level. The equation for his model states that

$$\left(\frac{4\pi a^2}{2}\right)\left[\sigma T_e^4\right] = \frac{\pi a R T_2 p_s}{gm}\left(1 - \frac{\gamma}{\gamma_d}\right)v_1 , \qquad (20)$$

where
- a = radius of Venus,
- p_s = surface pressure,
- γ = vertical temperature gradient,
- γ_d = g/c_p = adiabatic temperature gradient,
- T_2 = $(T_1 + T_3)/2$ = temperature at middle level of the atmosphere,
- $(\ )_{1,2,3}$ = subscripts referring to the different levels of the atmosphere; Level 1 refers to the level at which pressure is 1/4 of surface pressure, p_s; Level 2 refers to the level at which $p = 1/2\ p_s$, etc.,
- σ = Stefan-Boltzmann constant,
- R/m = gas constant for atmosphere with molecular weight, m,
- g = gravitational acceleration,
- T_e = infrared brightness temperature,
- v_1 = velocity at pressure surface $1/4\ p_s$ at terminator.

The left hand side of the formula represents the outgoing energy in the dark hemisphere and the right hand side represents the energy that must be transported from the sunlit side. With the following data

$p_s = 10$ atm. $\qquad$ $R/m = 3 \times 10^6$ cm^2/sec^2/deg

$T_2 = 580^oK$ $\qquad$ $a = 6 \times 10^6$ m

$T_e = 237^{\circ}K$ [23] $\qquad g = 8.4\ m/sec^2$

$\gamma/\gamma_d = 9/10$ $\qquad \sigma = 5.7 \times 10^{-5} erg/cm^2/sec/deg^4$,

one obtains the velocity at level $3p_s/4$ to be

$$v_3 = -1.0\ m/sec\ , \tag{21}$$

where the negative sign represents a wind direction toward the subsolar point. If we extrapolate to the surface, the wind velocity would be twice this value, or

$$v_4 = -2.0\ m/sec\ . \tag{22}$$

It is noticed that this mean wind velocity is relatively small as compared to the value $v \approx 8$ m/sec, obtained with $k = 5 \times 10^{-5}$/sec in Haurwitz's model. To find a representative estimate of the mean surface wind velocity, we must test and compare the results of all available models of the general circulation.

Linearized general circulation models. — Three circulation models are used to study the general circulation of Venus in detail. Each model assumes that the circulation starts from relative rest. Model 1 is based on a two-dimensional heating function which causes atmospheric motion. Both Model 2 and Model 3 assume that an uneven surface temperature distribution causes atmospheric circulation; the former model uses the Boussinesq approximation and the latter one assumes a compressible atmosphere. Vertical profiles of wind and temperature fields are computed from these models and are compared with the calculations of the previous section.

Model 1. — The following model of the circulation is based on a driving force due to a net gain of radiation energy at the subsolar point and a loss of radiation energy at the antisolar point. A two-dimensional linear model is used — that is, the circulation is represented on a vertical plane extending from the subsolar point to antisolar point and the planet's curvature is neglected. Since the effect of rotation of Venus is negligible, motion is mainly in the meridional direction (here we define the meridional direction in the direction of lines joining the subsolar and antisolar points). To keep the mathematics tractable, the motion is assumed to start from relative rest. Then, the equation of motion, energy equation, and equation of continuity can be simply written as

$$-\nu\nabla^2 v = -\frac{\partial\phi}{\partial y}\ , \tag{23}$$

$$\frac{\partial\phi}{\partial p} = -\frac{RT}{p}\ , \tag{24}$$

$$- \kappa\nabla^2 T + \Gamma\omega = \frac{Q}{c_p} \quad , \tag{25}$$

$$\frac{\partial v}{\partial y} + \frac{\partial \omega}{\partial p} = 0 \quad , \tag{26}$$

where Q = non-adiabatic net heating,
c_p = specific heat at constant pressure,
ν, κ = eddy viscosity and eddy heat conductivity respectively, (here we assume $\nu/\kappa = 1$),
v = velocity in the meridional direction (in y-direction),
ω = dp/dt = vertical velocity in pressure coordinates system,
T, p = temperature and pressure, respectively,
∇^2 = Laplacian operator,
Φ = geopotential height,
R = gas constant for Venusian atmosphere
Γ = stratification factor = $\frac{T}{\theta}\frac{\partial\theta}{\partial p} = \frac{\partial T}{\partial p} + (\frac{\Gamma_d}{\partial p/\partial z})$ (as a first approximation, Γ is assumed to be $-B_o/p_o$ where B_o is the temperature difference between the surface and the top of the atmosphere),
Γ_d = dry adiabatic lapse rate,
θ = potential temperature.

From the equation of continuity (26), we may write

$$v = \frac{\partial \psi}{\partial p}$$

and (27)

$$\omega = - \frac{\partial \psi}{\partial y}$$

where ψ = stream function. Substituting Equation (27) into (23) and (25) and eliminating Φ by using Equation (24), we obtain

$$- \frac{p}{R} \nu\nabla^2 \frac{\partial^2 \psi}{\partial p^2} = \frac{\partial T}{\partial y} \tag{28}$$

and

$$-\Gamma \frac{\partial^2 \psi}{\partial y^2} - \nu\nabla^2 \frac{\partial T}{\partial y} = \frac{\partial Q}{\partial y} \frac{1}{c_p} \quad . \tag{29}$$

If we approximate the eddy viscosity and heat conductivity by Rayleigh friction and Newtonian conductivity, i.e., by replacing $\nu\nabla^2$ by -c, and eliminating T from Equation (28) and (29), we obtain

$$-\Gamma \frac{\partial^2 \psi}{\partial y^2} + \frac{c^2 p}{R} \frac{\partial^2 \psi}{\partial p^2} = \frac{\partial Q/\partial y}{c_p} \quad . \tag{30}$$

Let $q = 2\left(\frac{p}{p_o}\right)^{1/2}$ and $\Gamma = -\frac{B_o}{p_o}$.

Equation (30) can be then written as

$$\frac{\partial^2 \psi}{\partial y^2} + \frac{c^2}{RB_o}\left(\frac{\partial^2 \psi}{\partial q^2} - \frac{1}{q}\frac{\partial \psi}{\partial q}\right) = \frac{p_o}{c_p B_o}\frac{\partial Q}{\partial y} \quad . \tag{31}$$

Let the net non-adiabatic heating, Q, as a function of latitude and pressure, be represented by

$$Q = DqJ_1(\alpha q)\left[N(y) - \frac{W}{aD}\right] ,$$

where $$D = S(1-A)\Big/\int_o^{p_o} qJ_1(\alpha q)\,\frac{dp}{g} ,$$

$$a = \int_o^{p_o} qJ_1(\alpha q)\,\frac{dp}{g} ,$$

S = the solar constant at Venus' distance from the sun,
A = the planetary albedo,
$q = 2\left(\frac{p}{p_o}\right)^{1/2}$,
$\alpha = 1.916$,
p, p_o = pressure and surface pressure respectively,
$DN(y)$ = variation of absorption of solar radiation as a function of latitude alone,
W = long-wave radiation is a constant over all horizontal surfaces,
J_1 = Bessel function of the first kind of order one.

Further let

$$\psi = DqJ_1(\alpha q)f,$$

f = the horizontal distribution of stream function.

In the above definitions, the vertical profile of the net energy is assumed proportional to $qJ_1(\alpha q)$ and the horizontal distribution is assumed proportional to $[N-(W/aD)]$ where N is assumed as a cosine function between y = 0 and y = L/2 and zero between y = L/2 to y = L as shown in Figure 11.

Substituting ψ and Q into Equation (31) and letting $(\pi/L)y = \varphi$ (φ representing the angle between subsolar point and any point on the surface along the meridional direction), one obtains

$$\frac{\partial^2 f}{\partial \varphi^2} - \mu f = \lambda \frac{\partial}{\partial \varphi} \left[N - \frac{W}{aD}\right] \quad , \tag{32}$$

where $\mu = \dfrac{\alpha^2 c^2 a^2}{RB_o}$, $\lambda = \dfrac{p_o a}{B_o c_p}$.

The function N can be approximated by a Fourier cosine series in a range between 0 and π

$$N = \frac{a_o}{2} + \sum_{\ell=1}^{\infty} a_\ell \cos \ell\varphi \quad , \tag{33}$$

where $\dfrac{a_o}{2} = \dfrac{1}{\pi}$,

$a_1 = 1/2$,

$$a_{\ell=2m} = \sum_{m=1}^{\infty} \frac{2(-1)^{m+1}}{(4m^2-1)\pi} \cos 2m\varphi \quad , \qquad \text{at } \ell \geq 2m.$$

The function f in ψ can be assumed as a Fourier sine series

$$f = \frac{2}{\pi} \sum_{n=1}^{\infty} b_n \sin n\varphi \quad . \tag{34}$$

Substituting (33) and (34) into Equation (32), then multiplying sin $n\varphi$ and integrating φ from 0 to π, one obtains

$$-(n^2 + \mu)b_n = -\lambda n \left\{ \frac{\pi}{4}\delta + \sum_{m=1}^{\infty} \frac{(-1)^{m+1}}{(4m^2-1)} \right\}$$

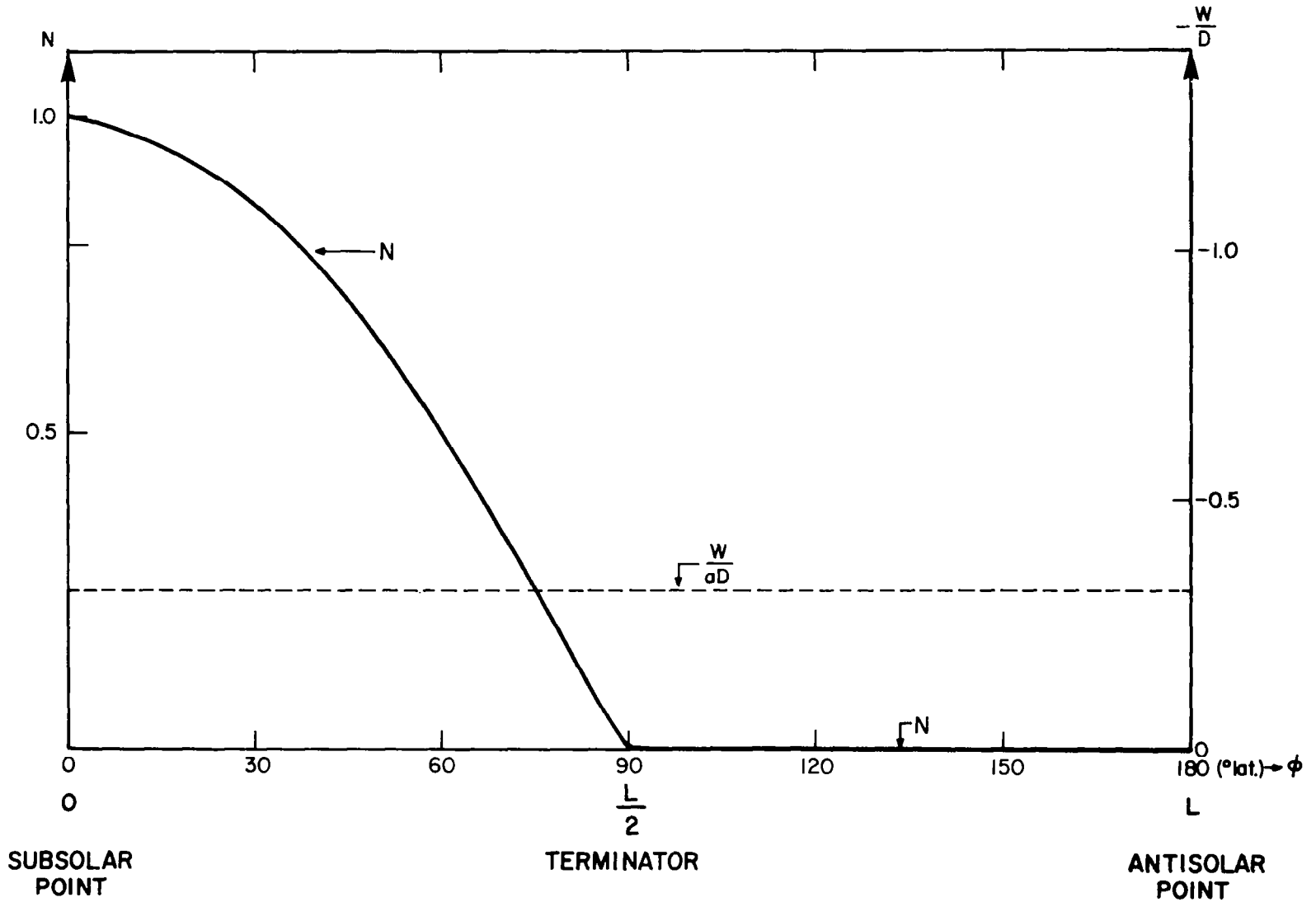

Figure 11. Horizontal distribution of N and W/aD.

or

$$b_n = \frac{\lambda n}{n^2+\mu}\left\{\frac{\pi}{4}\delta + \sum_{m=1}^{\infty}\frac{(-1)^{m+1}}{(4m^2-1)}\right\}; \tag{35}$$

$$\delta = \begin{cases} 0 \ , \ n \neq 1 \\ 1 \ , \ n = 1 \ . \end{cases}$$

More explicitly

$$b_1 = \frac{\lambda}{1+\mu}\frac{\pi}{4}$$

$$b_2 = \frac{2\lambda}{3(4+\mu)}$$

$$b_4 = -\frac{4\lambda}{15(16+\mu)}$$

$$b_6 = \frac{6\lambda}{35(36+\mu)}$$

.

.

.

Therefore, the stream function ψ and velocity v can be written as

$$\psi = 2D\left(\frac{p}{p_o}\right)^{\frac{1}{2}} J_1\left[2\alpha\left(\frac{p}{p_o}\right)^{\frac{1}{2}}\right]\frac{2}{\pi}\left\{\frac{\pi}{4}\frac{\lambda}{1+\mu}\sin\varphi + \frac{2\lambda}{3(4+\mu)}\sin 2\varphi - \frac{4\lambda}{15(16+\mu)}\sin 4\varphi + \right.$$

$$\left. + \frac{6\lambda}{35(36+\mu)}\sin 6\varphi - \frac{8\lambda}{63(64+\mu)}\sin 8\varphi + \ldots\ldots\ldots\right\} \tag{36}$$

and

$$v = \frac{\partial \psi}{\partial p} = \frac{2\alpha D}{p_o} J_o \left[2\alpha \left(\frac{p}{p_o}\right)^{\frac{1}{2}}\right] \frac{2}{\pi} \left\{ \frac{\pi}{4} \frac{\lambda}{1+\mu} \sin \varphi + \frac{2\lambda}{3(4+\mu)} \sin 2\varphi - \right.$$

$$\left. - \frac{4\lambda}{15(16+\mu)} \sin 4\varphi + \ldots\ldots\ldots\ldots \right\} . \qquad (37)$$

At the terminator, i.e., $\varphi = \pi/2$, Equation (37) becomes

$$v = \frac{D\alpha}{p_o} J_o \left[2\alpha \left(\frac{p}{p_o}\right)^{\frac{1}{2}}\right] \frac{\lambda}{1+\mu} \quad . \qquad (38)$$

Assuming a solar constant of 4.11 cal/cm^2/min and an albedo of 0.75 the quantity D in Equation (38) is about 3.5×10^{-6} cal/gm/sec. Together with the other constants used in a previous section, the computed wind velocities for $c = 10^{-5}$/sec and mean lapse rate of 8°C/km is 1.10 m/sec and for a lapse rate of 5°C/km is 2.75 m/sec. These values are in close agreement with the calculations using Mintz's model.

The horizontal distribution of v with latitude of the model (up to second harmonics) is shown in Figure 12. The stream function is plotted in Figure 13. It is seen that the maximum surface velocity is not at the terminator but on the sunlit side at somewhere between 60° and 70° latitude on our scale. The center of the vertical circulation is also located at the same latitude and the circulation is not symmetrical. The asymmetry of the circulation is probably due to the asymmetry of the gradient of the non-adiabatic heating. This asymmetry probably causes a strong upward flux of heat in the area immediately surrounding the subsolar point. Since no net energy can be retained in a horizontal slice, the area of upward motion is smaller than the area of downward motion. As to the asymmetry in the vertical direction, it is mainly related to the vertical profile of the non-adiabatic heating function, Q, which we assumed to be asymmetrical for mathematical simplicity. Further investigation of the radiational heating function in the Venusian atmosphere is necessary. If the maximum intensity of the heating function is shifted downward in the atmosphere, then the entire circulation pattern would also shift downwards.

Model 2. — Since data are available on the temperature variation between subsolar and antisolar points, we can estimate the average wind velocities using the Boussinesq approximation for a free convection model. This approach has been used successfully for model circulation systems in which rotation effects are unimportant and the systems are relatively shallow, such as the circulation patterns associated with land and sea, or valley and mountain circulations. Although the troposphere of Venus' atmosphere may be rather thick, it would be interesting to compare the computed results using this approach with the other calculations.

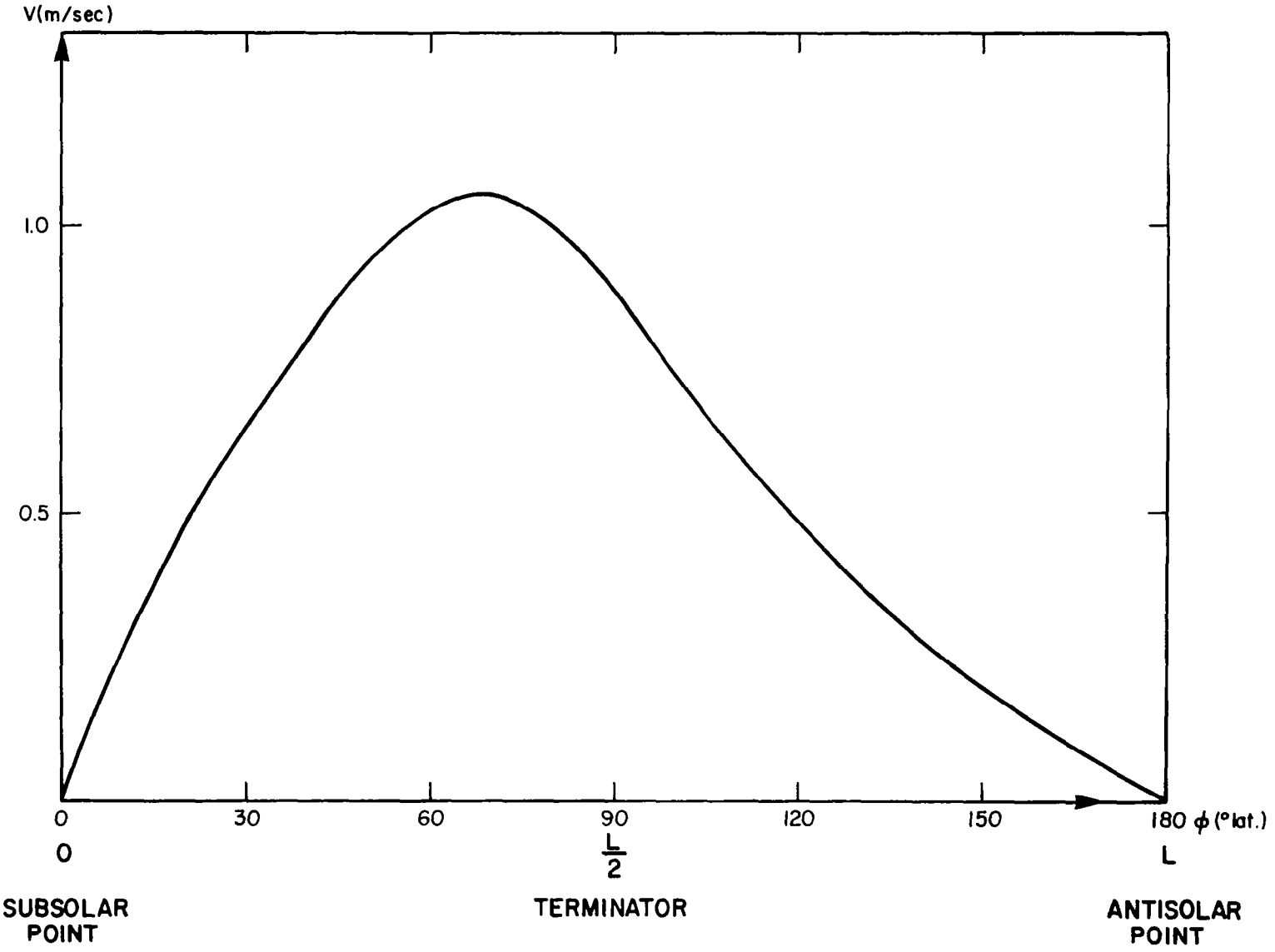

Figure 12. Horizontal distribution of velocity v with latitude.

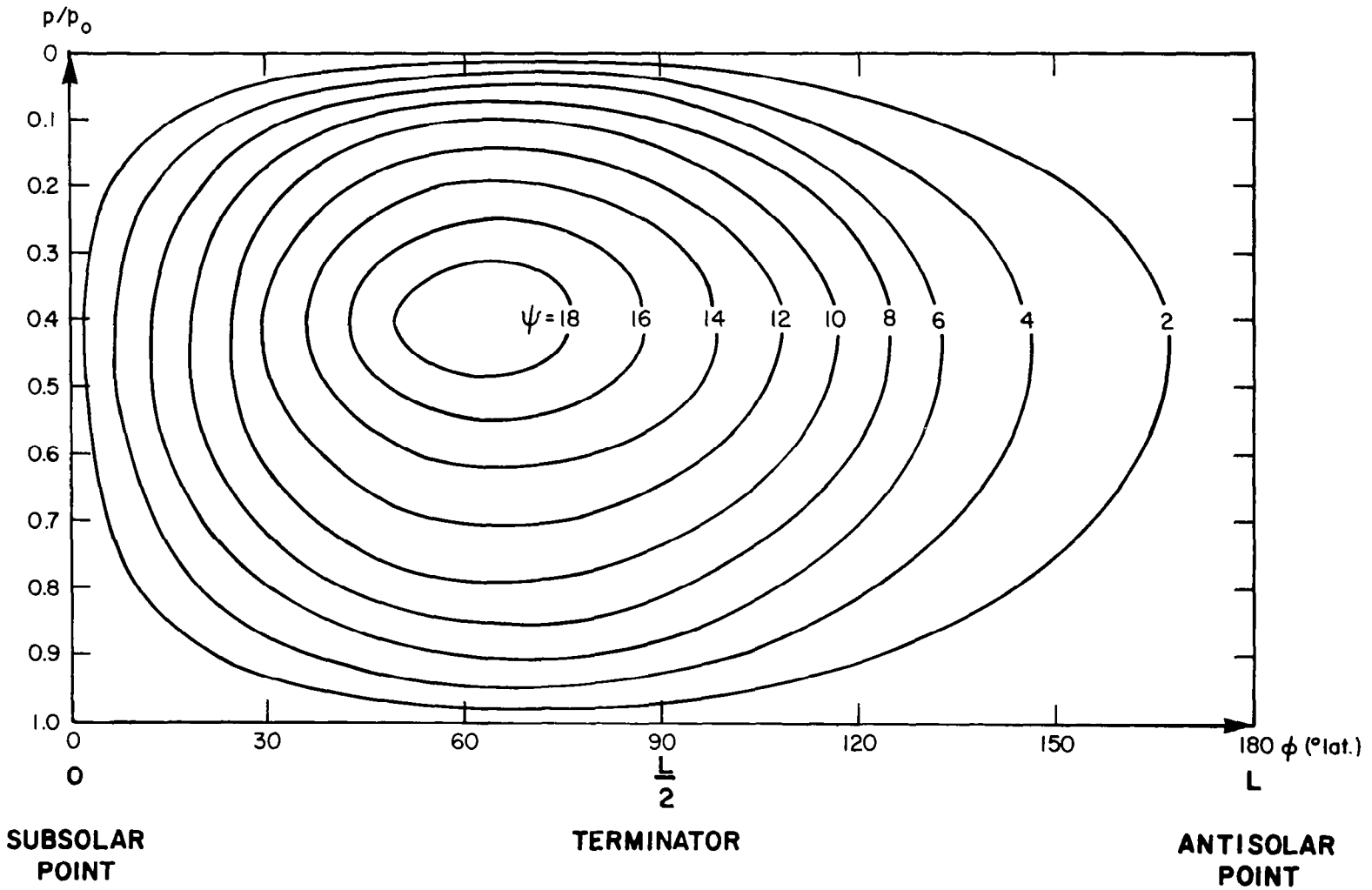

Figure 13. Stream field (ψ is in unit of 2.33×10^{-8} gm sec^{-3}).

Let us assume the temperature $\mathbb{T}$ is given by

$$\mathbb{T} = \overline{\mathbb{T}}(x,z) + T(x,z) \quad , \tag{39}$$

where $\overline{\mathbb{T}}$ = mean temperature = $\mathbb{T}_o - \gamma_m z$,

$\mathbb{T}_o$ = mean surface temperature,

T = perturbation temperature,

γ_m = mean lapse rate,

x,z = horizontal distance from subsolar point and height from surface respectively.

The heat equation can be written as

$$\left(\frac{\partial}{\partial t} + U \frac{\partial}{\partial x} \right) \mathbb{T} + W \left(\frac{\partial \mathbb{T}}{\partial z} + \Gamma_d \right) = \kappa \nabla^2 \mathbb{T} \ , \tag{40}$$

where U,W = total horizontal and vertical velocities,

Γ_d = dry adiabatic lapse rate,

∇^2 = two-dimensional Laplacian operator,

κ = coefficient of eddy conductivity

Let the mean lapse rate γ_m be a linear function of x, then

$$\gamma_m = \gamma_o(1 + bx) \ , \tag{41}$$

where b is a constant and γ_o is the mean lapse rate at $x = 0$. Let

$$U = \overline{U} + u$$

$$W = \overline{W} + w \ ,$$

where $\overline{U}$ and $\overline{W}$ are mean horizontal and vertical velocities respectively and u and w are the corresponding perturbation quantities.

Starting from rest, $\overline{U} = \overline{W} \approx 0$. From Equation (40) the perturbation equation for T in the steady state becomes

$$\kappa \nabla^2 T = [\Gamma_d - \gamma_o(1 + bx)]w - \gamma_o(bz)u \quad . \tag{42}$$

Using the Boussinesq approximation [27], we obtain the following steady state *perturbation equations for horizontal and vertical motion*

$$- \nu\nabla^2 u = - \frac{1}{\rho} \frac{\partial p}{\partial x} \quad , \tag{43}$$

$$- \nu\nabla^2 w = - \frac{1}{\rho} \frac{\partial p}{\partial z} + g\alpha T \quad , \tag{44}$$

and equation of continuity

$$\frac{\partial u}{\partial x} + \frac{\partial w}{\partial z} = 0 \quad , \tag{45}$$

where u,w = perturbed velocities along x and y direction, respectively,
p,T = perturbed pressure and temperature, respectively,
ρ = mean density,
α = *coefficient of expansion of the gas.*

Eliminating p between Equations (43) and (44) and using (45) yields

$$\nu\nabla^4 u = g\alpha \frac{\partial^2 T}{\partial x \partial z} \quad , \tag{46}$$

$$- \nu\nabla^4 w = g\alpha \frac{\partial^2 T}{\partial x^2} \quad , \tag{47}$$

From the equation of continuity (45) we obtain the stream function

$$u = \psi_z \qquad \text{and} \qquad w = -\psi_x \quad . \tag{48}$$

It follows that Equations (46), (47) and (48) can be written as

$$\nu\nabla^4 \psi_z = g\alpha \frac{\partial^2 T}{\partial x \partial z} \quad , \tag{49}$$

$$\nu\nabla^4 \psi_x = g\alpha \frac{\partial^2 T}{\partial x^2} \quad , \tag{50}$$

$$\kappa\nabla^2 T = - \gamma_o [(\frac{\Gamma_d}{\gamma_o} - (1 + bx))\psi_x + bz\psi_z] \quad . \tag{51}$$

From Equations (49), (50), and (51) we obtain

$$\Delta^3\psi = \frac{g\alpha\gamma_o}{\nu K}\left[-\left(\frac{\Gamma_d}{\gamma_o} - (1 + bx)\right)\psi_{xx} + b\psi_x - bz\psi_{xz}\right] , \tag{52}$$

and

$$\Delta^4 T = \frac{g\alpha\gamma_o}{\nu K}\left\{-\Delta\left[\left(\frac{\Gamma_d}{\gamma_o} - (1 + bx)\right)T_{xx}\right] - b\Delta(zT_{xz}) + 4b(T_{xxx} - T_{xzz})\right\} \tag{53}$$

where $\Delta = \nabla^2$ = Laplacian.

If the lapse rate is independent of location, then Equations (52) and (53) reduce to

$$\Delta^3\psi = -\frac{g\alpha\gamma}{\nu K}\psi_{xx} , \tag{54}$$

$$\Delta^3 T = -\frac{g\alpha\gamma}{\nu K} T_{xx} , \tag{55}$$

respectively, where $\gamma = \Gamma_d - \gamma_o$. For the average case, the mean lapse rate, γ_o, is less than dry adiabatic; thus

$$\gamma > 0 .$$

In the earth's atmosphere, γ is approximately $4^oC/km$.

The differential Equations (54) and (55) are rather tractable and are solved easily if the boundary conditions are known. These solutions would be a first approximation to the actual atmospheric circulation. Since the differential equations have constant coefficients, the solutions for Equations (54) and (55) can be expressed by a Fourier series.

First we determine the temperature in Equation (55) and use it to determine the stream function or velocity field. The Fourier solution for the temperature T is

$$T = C\, e^{mz} \cos kx ,$$

where C = amplitude of temperature disturbance,
$k = \pi/L$,
L = the distance between subsolar and antisolar points.

Substituting this solution into Equation (55), we have

$$(\alpha^* - 1)^3 - \beta^3 = 0 \ , \tag{56}$$

where $\alpha^* = m^2/k^2$ and $\beta = (\frac{g\alpha\gamma}{\nu\kappa}/k^4)^{1/3}$. The algebraic equation (56) has three possible solutions, which are

$$\left.\begin{aligned} \alpha_1^* &= 1 + \beta \\ \alpha_2^* &= 1 - \tfrac{1}{2}(1 + \sqrt{3}i)\beta \\ \alpha_3^* &= 1 - \tfrac{1}{2}(1 - \sqrt{3}i)\beta \ . \end{aligned}\right\} \tag{57}$$

If we let

$$\begin{aligned} g &= 8.8 \text{ m/sec}, \\ \alpha &= 1/500 = 0.002/\text{deg}, \\ \Gamma_d &= 9^\circ\text{C/km}, \\ \gamma_o &= 7^\circ\text{C/km}, \end{aligned}$$

and

$$\nu = \kappa = 10^3 \text{ m}^2/\text{sec},$$

then

$$\beta \approx 3.6 \times 10^5 \ ,$$

which is much larger than unity. Then

$$\left.\begin{aligned} m_1 &\cong -\lambda k \\ m_2 &\simeq (-\tfrac{1}{2} + .866i)\lambda k \\ m_3 &\simeq (-\tfrac{1}{2} - .866i)\lambda k \ , \end{aligned}\right\} \tag{58}$$

where $\lambda = \sqrt{\beta}$. Here only the negative roots are taken, since the temperature perturbation at the top of the atmosphere is finite.

The solution for temperature, T, can be written as

$$T = \sum_{i=1}^{3} C_i e^{m_i z} \cos kx \ . \tag{59}$$

Similarly, the following solutions can be assumed for w and u:

$$w = A\ e^{mz} \cos kx \ ,$$

and

$$u = B\ e^{mz} \cos kx \ .$$

Applying the boundary condition that $w = u = 0$ at $z = 0$, we have

$$\sum_{i=1}^{3} A_i = 0 \ , \tag{60}$$

and

$$\sum_{i=1}^{3} A_i m_i = 0 \tag{61}$$

for w and u respectively. Similarly, an additional relation for perturbation temperature is

$$\frac{\gamma}{\kappa} \sum_{i=1}^{3} \left(\frac{A_i}{m_i^2 - k^2} \right) = D \ , \tag{62}$$

where D is the amplitude of the temperature disturbance. With Equations (60), (61), and (62) we can solve for the coefficients A_1, A_2 and A_3 as follows

$$A_1 = \frac{\kappa D}{\gamma \Delta} (m_2 - m_3)$$

$$A_2 = \frac{\kappa D}{\gamma \Delta} (m_3 - m_1)$$

$$A_3 = \frac{\kappa D}{\gamma \Delta} (m_1 - m_2) ,$$

where
$$\Delta = \begin{vmatrix} 1 & 1 & 1 \\ m_1 & m_2 & m_3 \\ \frac{1}{m_1^2 - k^2} & \frac{1}{m_2^2 - k^2} & \frac{1}{m_3^2 - k^2} \end{vmatrix} .$$

Then the solution for u, w, and T can be written as

$$u = \frac{\kappa D}{\gamma \Delta} \frac{1}{k} \left[m_1 (m_2 - m_3) e^{m_1 z} + m_2 (m_3 - m_1) e^{m_2 z} + m_3 (m_1 - m_2) e^{m_3 z} \right] \sin kx, \qquad (63)$$

$$w = \frac{\kappa D}{\gamma \Delta} \left[(m_2 - m_3) e^{m_1 z} + (m_3 - m_1) e^{m_2 z} + (m_1 - m_2) e^{m_3 z} \right] \cos kx , \qquad (64)$$

$$T = \frac{D}{\Delta} \left[\frac{m_3 - m_2}{m_1^2 - k^2} e^{m_1 z} + \frac{m_1 - m_3}{m_2^2 - k^2} e^{m_2 z} + \frac{m_2 - m_1}{m_3^2 - k^2} \right] \cos kx. \qquad (65)$$

Substituting m_1, m_2 and m_3 from Equation (58) into (63), (64) and (65) and taking the real part of the solution, we have

$$u = \frac{\kappa \lambda^3 k^2 D}{2\gamma} \left\{ e^{-\lambda k z} - \left[\cos \sqrt{\frac{3}{2}} \lambda k z + \sqrt{\frac{3}{3}} \sin \sqrt{\frac{3}{2}} \lambda k z \right] e^{-\frac{\lambda k z}{2}} \right\} \sin kx , \qquad (66)$$

$$w = \frac{\kappa D (\lambda k)^2}{2\gamma} \left\{ e^{-\lambda k z} - \left[\cos \sqrt{\frac{3}{2}} \lambda k z - \sqrt{\frac{3}{3}} \sin \sqrt{\frac{3}{2}} \lambda k z \right] e^{-\frac{\lambda k z}{2}} \right\} \cos kx , \qquad (67)$$

$$T = \frac{D}{2} \left\{ e^{-\lambda k z} + \cos \left(\sqrt{\frac{3}{2}} \lambda k z \right) e^{-\frac{\lambda k z}{2}} \right\} \cos kx , \qquad (68)$$

where D = amplitude of temperature disturbance,

$\kappa = \nu$ = eddy conductivity or viscosity,

$k = 1/r_o$,

r_o = radius of Venus,

$\lambda = \left[\frac{g\alpha\gamma}{\nu\kappa} \Big/ k^4 \right]^{1/6}$.

The surface temperature distribution on Venus [28] is

$$T = [621 + 73 \cos(\varphi + 11.7)]^{\circ}K , \tag{69}$$

where φ is the phase angle. The above expression can be thought of as representing the temperature variation from subsolar to antisolar points on the planet with φ representing the angle between subsolar point and any point on the surface along the meridional direction. If we neglect the phase shift angle of 11.7°, the perturbation temperature becomes a cosine function with an amplitude, D, $73^{\circ}K$. This tractable equation is the desired solution.

For $\kappa = \nu = 10^3$ m^2/sec

$g = 8.8$ m/sec^2

$D = 73^{\circ}K$

$r_o = 6100$ km

$k = 1.64 \times 10^{-4}$/km

$\alpha = 0.002$/deg

$\gamma = 2^{\circ}$/km

$\lambda = 605$,

the computed horizontal and vertical wind velocities, and the perturbation temperature are plotted as a function of height in Figure 14.

From Figure 14 it is seen that the maximum horizontal wind velocity is about 35 m/sec and is located approximately at 8 km above the solid surface in the direction toward subsolar point. The maximum return flow is about 20 m/sec at 35 km above surface in the direction toward antisolar point. The computed maximum vertical velocity is about 2.0 cm/sec and is located at 28 km; the vertical velocity decreases to zero at 50 km above the surface. The perturbation temperature decreases upwards from the surface to a minimum at 30 km and then remains approximately constant.

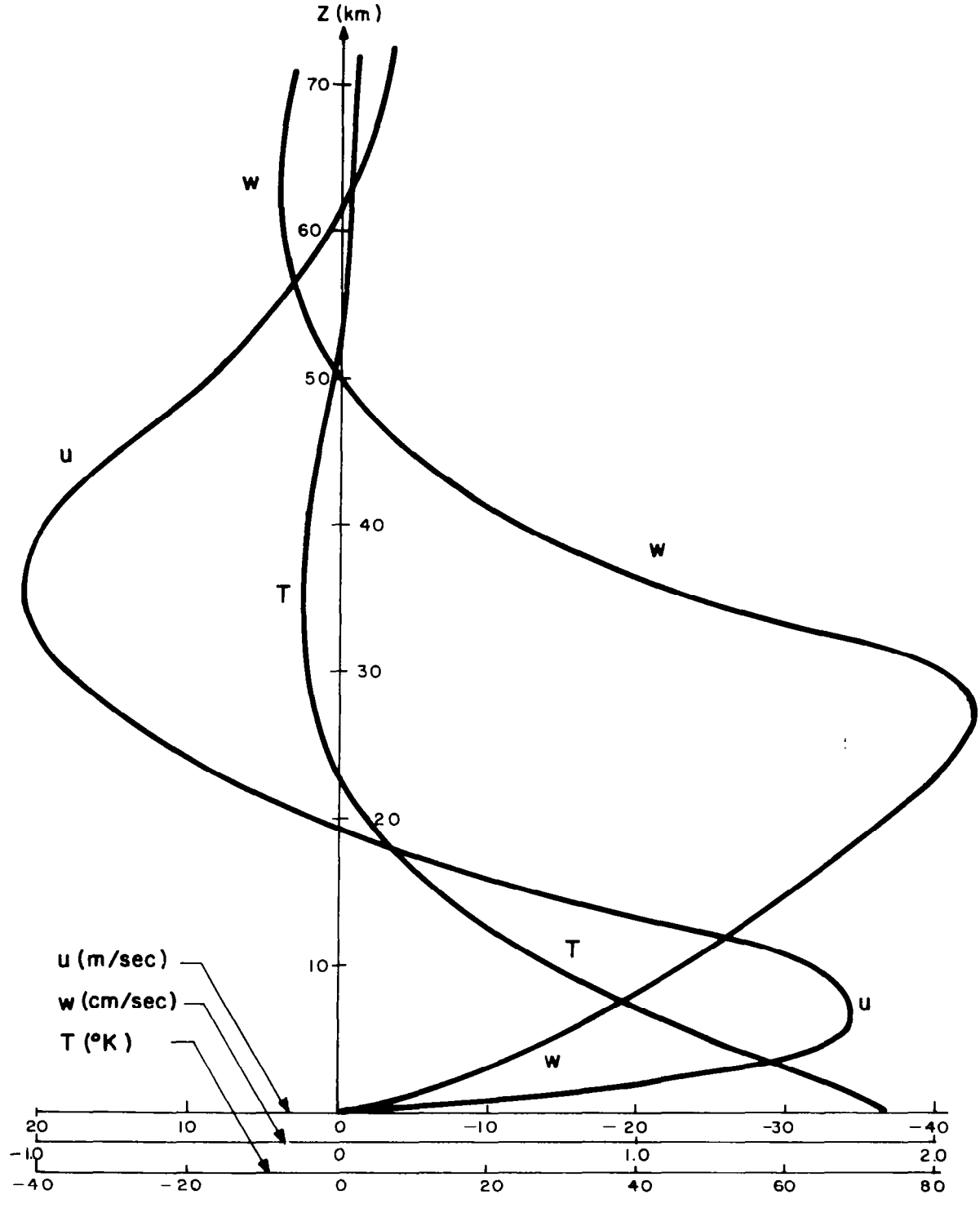

Figure 14. Computed horizontal and vertical wind velocities (u and w) and perturbation temperature (T) for Venus atmosphere ($\kappa = \nu = 10^3 m^2/sec$, $g = 8.8$ m/sec^2; $D = 73^oK$; $r = 6100$ km; $k = 1.64^{-4}$/km; $\alpha = 0.002$; $\gamma = 2^o$/km; $\lambda = 605$; $\varphi = \pi/2$ for u, and $\varphi = 0$ for w and T).

The computations show that upward vertical velocities extend to 50 km on the sunlit side of the planet, and downward vertical velocities extend 50 km on the dark side of the planet. Since upward vertical velocities may extend to 50 km, clouds may extend to this same altitude.

Model 3. — In Model 2 we studied the general circulation problem under the Boussinesq approximation as an experiment. This approximation means that the fluctuation in density which appears with the advent of motion results principally from thermal (as opposed to pressure) effects and that density variations may be neglected in the equations of motion and continuity except when density variations are coupled to the acceleration of gravity in the buoyancy force. Models using this approximation are generally successful when they are applied to a relatively shallow layer of fluid in a convective problem. As to a thick atmosphere, the Boussinesq approximation would lead to larger errors.

Model 3 retains the convective model, but the simple Boussinesq approximation is abandoned. Then a more realistic result may be obtained, which can be compared with the results obtained earlier.

Let subscript o denote the unperturbed quantities at a level, and s, at the surface. Then we can write the temperature, pressure, and density for a steady state as

$$T_o(x,y,z) = T_s(x,y) - \gamma z \tag{70}$$

$$P_o(x,y,z) = p_s(x,y)\left(1 - \frac{\gamma z}{T_s}\right)^{\frac{1}{K_*}} \tag{71}$$

$$\rho_o(x,y,z) = \frac{p_s \gamma K_*}{g T_s}\left(1 - \frac{\gamma z}{T_s}\right)^{\frac{1-K_*}{K_*}} \tag{72}$$

respectively, where γ = lapse rate,

K_* = 0.288, if the lapse rate of the atmosphere is dry adiabatic; otherwise, non-adiabatic lapse rate $K_* = f(\gamma)$,

g = acceleration of gravity.

For rectangular coordinates the equations of motion, energy, continuity, and state can be written as

$$\rho \frac{du}{dt} = -\frac{\partial P}{\partial x} + \rho\left(\nu_h \frac{\partial^2 u}{\partial x^2} + \nu_v \frac{\partial^2 u}{\partial z^2}\right) \tag{73}$$

$$\rho \frac{dw}{dt} = - \frac{\partial P}{\partial z} + g\rho \left(\nu_h \frac{\partial^2 w}{\partial x^2} + \nu_v \frac{\partial^2 w}{\partial z^2} \right) , \tag{74}$$

$$\rho c_v \frac{dT}{dt} + P \left(\frac{\partial u}{\partial x} + \frac{\partial w}{\partial z} \right) = \left(k_h \frac{\partial^2 T}{\partial x^2} + k_v \frac{\partial^2 T}{\partial z^2} \right) , \tag{75}$$

$$\frac{\partial \rho}{\partial t} + u \frac{\partial \rho}{\partial x} + w \frac{\partial \rho}{\partial z} + \rho \left(\frac{\partial u}{\partial x} + \frac{\partial w}{\partial z} \right) = 0 , \tag{76}$$

$$P = \rho RT , \tag{77}$$

respectively, where

P = total pressure,
ρ = total density,
T = total temperature,
u,w = total velocity components along x and y direction (assume the origin of the coordinates at the subsolar point; x is the distance from subsolar point; z points upward),
ν_h, ν_v = coefficients of eddy viscosity in horizontal and vertical directions, respectively,
k_h, k_v = kinematic coefficients of eddy conductivity in horizontal and vertical directions, respectively,
c_v = specific heat at constant volume.

Assume the basic state to be relatively at rest and let the non-subscript dependent variables denote the small deviation from steady state hereafter. The perturbation Equations (73) to (76) for the steady state case are then

$$-\rho_o \left(\nu_h \frac{\partial^2 u}{\partial x^2} + \nu_v \frac{\partial^2 u}{\partial z^2} \right) = - \frac{\partial p}{\partial x} , \tag{78}$$

$$- \rho_o \left(\nu_h \frac{\partial^2 w}{\partial x^2} + \nu_v \frac{\partial^2 w}{\partial z^2} \right) = - \frac{\partial p}{\partial z} + g\rho , \tag{79}$$

$$w \frac{\partial T_o}{\partial z} + (\lambda - 1) T_o \left(\frac{\partial u}{\partial x} + \frac{\partial w}{\partial z} \right) = K_h \frac{\partial^2 T}{\partial x^2} + K_v \frac{\partial^2 T}{\partial z^2} , \tag{80}$$

$$w \frac{\partial \rho_o}{\partial z} + \rho_o \left(\frac{\partial u}{\partial x} + \frac{\partial w}{\partial z} \right) = 0 , \tag{81}$$

$$\frac{T}{T_o} = \frac{p}{P_o} - \frac{\rho}{\rho_o} \quad , \tag{82}$$

where

$$K_h, K_v = \frac{c_p}{c_v} K_{h*}, \frac{c_p}{c_v} K_{v*} \ ,$$

$K_{h*}, K_{v*} = \left(\frac{k_h}{c_p \rho_o} \right), \left(\frac{k_v}{c_p \rho_o} \right)$ = coefficients of eddy conductivity in horizontal and vertical respectively,

$$\lambda = \frac{c_p}{c_v} = \frac{R}{c_v} + 1 \ ,$$

c_p = specific heat at constant pressure.

Now assume the solutions for the last set of Equations (78) to (82) are

$$[w, T, p, \rho] = [\hat{w}(z), \hat{T}(z), \hat{p}(z), \hat{\rho}(z)] \cos bx \ , \tag{83}$$

$$u = \hat{u}(z) \sin bx \quad . \tag{84}$$

Substituting Equations (83) and (84) into (78) to (82) and assuming $\nu_h = K_h$, $\nu_v = K_v$ yields

$$-\rho_o \nu_v L\hat{u} = b\hat{p} \ , \tag{85}$$

$$-\rho_o \nu_v L\hat{w} = -D\hat{p} + g\hat{\rho} \ , \tag{86}$$

$$L\hat{T} = \phi\hat{w} \ , \tag{87}$$

$$\hat{w}/H = b\hat{u} + D\hat{w} \ , \tag{88}$$

$$\hat{T} = \alpha\hat{p} - \beta\hat{\rho} \ , \tag{89}$$

where $L = D^2 - \sigma b^2$,

$D = d/dz$,

$\sigma = \nu_h/\nu_v = \kappa_h/\kappa_v$,

$\alpha(z) = T_o/P_o$,

$\beta(z) = T_o/\rho_o$,

$$H = -\left(\frac{1}{\rho_o}\frac{\partial \rho_o}{\partial z}\right)^{-1},$$

$$\phi = \frac{1}{\kappa_v}\left[\frac{\partial T_o}{\partial z} + \frac{(\lambda - 1)T_o}{H}\right].$$

For brevity we drop off the hat for dependent variables and write ν_v or κ_v as ν hereafter. From Equations (85) and (88) one can obtain

$$\frac{\rho_o}{b^2}\nu L(Dw - \frac{w}{H}) = p \ . \tag{90}$$

After substituting Equation (89) into (90), one obtains

$$\frac{\rho_o \nu}{b^2} L(Dw - \frac{w}{H}) = \frac{T}{\alpha} + \frac{\beta}{\alpha}\rho \ . \tag{91}$$

By taking the derivative of p with respect to z in Equation (89) and substituting into (86) to eliminate Dp, one arrives at

$$-\rho_o \nu L w = L_1 T + L_2 \rho \ , \tag{92}$$

where $L_1 = \frac{D\alpha}{\alpha^2} - \frac{1}{\alpha} D$,

$L_2 = g - D(\beta/\alpha) - \frac{\beta}{\alpha} D$.

Eliminating ρ between Equations (91) and (92) yields

$$L_2\left[\frac{\rho_o\nu\alpha}{b^2\beta}\,L(Dw-\frac{1}{H}w)\right]+\rho_o\nu Lw=L_3T\ , \tag{93}$$

where $$L_3=L_2(1/\beta)+\frac{1}{\beta}\,L_2-L_1\ .$$

Further, eliminating w between Equations (86) and (93) one obtains the final governing equation for T as follows

$$L_2\left\{\frac{\rho_o\nu\alpha}{b^2\beta}\,L\left[D(\tfrac{1}{\phi}LT)-\frac{1}{H\phi}LT\right]\right\}+\rho_o\nu L(\tfrac{1}{\phi}LT)=L_3T\ , \tag{94}$$

or

$$-\left(\frac{\rho_o\nu}{b^2\phi}\right)\left(\frac{d^2}{dz^2}-\sigma b^2\right)\frac{d^2T}{dz^2}+\left\{\left[-\frac{\beta}{\alpha}\frac{d}{dz}\left(\frac{\rho_o\nu\alpha}{b^2\beta}\right)+\frac{\rho_o\nu}{b^2}\left(\frac{d\phi}{dz}\frac{1}{\phi^2}+\frac{1}{H\phi}\right)\right]\cdot\right.$$

$$\left.\cdot\left(\frac{d^2}{dz^2}-\sigma b^2\right)^2\frac{dT}{dz}-\left(\frac{2\rho_o\nu}{b^2}\frac{d}{dz}\frac{1}{\phi}\right)\left(\frac{d^2}{dz^2}-\sigma b^2\right)\frac{d^3T}{dz^3}\right\}\ +$$

$$+\left\{\left[\frac{\beta}{\alpha}\frac{d}{dz}\left(\frac{\rho_o\nu\alpha}{b^2\beta}\frac{1}{\phi^2}\frac{d\phi}{d\beta}+\frac{1}{H\phi}\right)+\frac{\rho_o\nu}{\phi}\right]\left(\frac{d^2}{dz^2}-\sigma b^2\right)^2T-\right.$$

$$-\left(-\frac{d}{dz}(\beta/\alpha)+g\right)\frac{\rho_o\nu\alpha}{b^2\beta}\left(\frac{1}{\phi^2}\frac{d\phi}{dz}+\frac{1}{H\phi}\right)\left(\frac{d^2}{dz^2}-\sigma b^2\right)^2T+$$

$$+\left[\frac{2\rho_o\nu}{b^2}\left(\frac{d}{dz}\frac{1}{\phi^2}\frac{d\phi}{dz}-\frac{d^2}{dz^2}\frac{1}{\phi}+\frac{d}{dz}\frac{1}{H\phi}\right)-\frac{\beta}{\alpha}\frac{d}{dz}\left(\frac{2\rho_o\nu\alpha}{b^2\beta}\frac{d}{dz}(1/\phi)\right)\right]\cdot$$

$$\left.\cdot\left(\frac{d^2}{dz^2}-\sigma b^2\right)\frac{d^2T}{dz^2}+\left(-\frac{d}{dz}(\beta/\alpha)+g\right)\left(\frac{2\rho_o\nu\alpha}{b^2\beta}\frac{d}{dz}\frac{1}{\phi}\right)\cdot\right.$$

$$\cdot \left(\frac{d^2}{dz^2} - \sigma b^2 \right) \frac{d^2 T}{dz^2} \Bigg\} + \Bigg\{ \frac{\beta}{\alpha} \frac{d}{dz} \Bigg[\frac{2\rho_o \nu \alpha}{b^2 \beta} \left(\frac{d}{dz} \frac{1}{\phi^2} \frac{d\phi}{dz} - \right.$$

$$\left. - \frac{d^2}{dz^2} (1/\phi) + \frac{d}{dz} \frac{1}{H\phi} \right) \Bigg] + 2\rho_o \nu \frac{d}{dz} \frac{1}{\phi} + \frac{\rho_o \nu}{b^2} \left(\frac{d^2}{dz^2} \frac{1}{\phi^2} \frac{d\phi}{dz} \right) +$$

$$+ \frac{d^2}{dz^2} \left(\frac{1}{H\phi} \right) \left(\frac{d^2}{dz^2} - \sigma b^2 \right) \frac{dT}{dz} + \left(- \frac{d}{dz} (\beta/\alpha) + g \right) \Bigg[\frac{2\rho_o \nu \alpha}{b^2 \beta} \cdot$$

$$\cdot \left(\frac{d}{dz} \left(\frac{1}{\phi^2} \frac{d\phi}{dz} \right) - \frac{d^2}{dz^2} \frac{1}{\phi} + \frac{d}{dz} \frac{1}{H\phi} \right) + \frac{\rho_o \nu \alpha}{b^2 \beta \phi} \Bigg] \left(\frac{d^2}{dz^2} - \sigma b^2 \right) \frac{dT}{dz} \Bigg\} +$$

$$+ \Bigg\{ \Bigg[\rho_o \nu \frac{d^2}{dz^2} \frac{1}{\phi} - \left(- \frac{d}{dz} (\beta/\alpha) + g \right) \frac{\rho_o \nu \alpha}{b^2 \beta} \left(\frac{d^2}{dz^2} \left(\frac{1}{\phi^2} \frac{d\phi}{dz} \right) + \frac{d^2}{dz^2} \frac{1}{H\phi} \right) \Bigg] \cdot$$

$$\cdot \left(\frac{d^2}{dz^2} - \sigma b^2 \right) T \Bigg\} - \Bigg\{ - \frac{1}{\alpha\beta} \frac{d\beta}{dz} + \frac{1}{\alpha^2} \frac{d\alpha}{dz} + \frac{2g}{\beta} \Bigg\} T = 0 \quad . \tag{95}$$

This is a sixth order ordinary differential equation. Six boundary conditions are needed. The conditions may be stated as follows:

(1) The amplitude of the temperature disturbance at the surface (z = 0) is assumed known and at the tropopause level (z = h) is zero.

(2) The velocities vanish both at the surface (z = 0) and at the tropopause level (z = h).

The first assumption yields

$$T = T_A \qquad \text{at } z = 0 \tag{96}$$

$$T = 0 \qquad \text{at } z = h \tag{97}$$

where T_A is the amplitude of the temperature disturbance. The second assumption, from Equation (87) and (88) leads to

$$(D^2 - \sigma b^2) T = 0 \qquad \text{at } z = 0 \text{ and } z = h \tag{98}$$

and

$$D\left[\frac{1}{\phi}(D^2 - \sigma b^2)T\right] = 0 \qquad \text{at } z = 0 \text{ and } z = h \qquad (99)$$

With all six boundary conditions, Equation (94) or (95) can be solved in principle. When this solution of T is obtained w can be obtained directly from Equation (87) and u, in turn from Equation (88).

Since the sixth order ordinary differential Equation (94) or (95) has very complicated variable coefficients, it is difficult to solve analytically. A numerical method is thus used for solving this equation.

The differential Equation (95) with the prescribed boundary conditions (96), (97), (98), and (99) can be solved numerically. Techniques for numerical solution are currently being examined.

Formation of Diverging Cloud Bands. — A radial spoke system of clouds has been observed on Venus (see Reference 29), but this observation has not been satisfactorily explained. Since Venus is nearly a synchronously rotating planet, the mean wind direction will be predominately in the meridional direction, between the subsolar and antisolar points. In the lower layers, the circulation is from the antisolar point to the subsolar point, and the flow converges radially toward the subsolar point. In the upper layer, the flow is in the opposite sense. This type of Hadley cell circulation leads to a mean vertical wind shear.

According to the study of vortex clouds in hurricanes [30] and related work [31], cloud bands tend to be oriented along the direction of flow. The meteorological conditions accompanying this phenomenon require that the atmosphere be unstably stratified and that the vertical wind shear be oriented along the direction of flow. It is probable that these conditions could occur in the lower layers of the Venusian atmosphere. Hence, the observation of radial spoke system appears to be in agreement with these theoretical considerations.

Discussion

Five models are used to study the circulation of the Venusian atmosphere. Mean wind speeds are computed from these models. The results are listed in Table 4.

The highest velocity, 33 m sec^{-1}, is obtained from the linearized Model 2. In this model the Boussinesq approximation is made. This approximation is not particularly appropriate for a thick atmosphere such as Venus'. The other models yield, using appropriate Venusian parameters, average wind speeds

TABLE 4

ESTIMATED SURFACE LEVEL WIND VELOCITIES IN THE VENUS ATMOSPHERE OBTAINED FROM DIFFERENT MODELS

Models	Velocity (m/sec)	Remarks
Haurwitz's Model	8	$\dot{c} = 5 \times 10^{-5}$/sec; at surface and tropopause level
	18	$c = 10^{-5}$/sec; at surface and tropopause level
Mintz's Model	2.0	$\frac{\partial T}{\partial z} = -8^{\circ}$/km; at surface and tropopause level
Linearized Model 1		$c = 10^{-5}$/sec, $\frac{\partial T}{\partial z} = -8^{\circ}$/km, maximum value at $\varphi \approx 70^{\circ}$ lat.
	1.10	at surface level;
	2.75	at top of the atmosphere
		$c = 10^{-5}$/sec, $\frac{\partial T}{\partial z} = -5^{\circ}$/km, maximum value at $\varphi \approx 70^{\circ}$ lat.
	0.20	at surface level;
	0.50	at top of the atmosphere
Linearized Model 2	33	$\nu = \kappa = 10^{7}$ cm^2/sec (maximum velocity is at 7 km above surface)

of 2-8 m sec^{-1}, which are believed to be more reliable estimates of Venusian velocities. These velocities are lower than average velocities in the earth's atmosphere. An improved linearized model — Model 3 — has been developed. It is planned to compare the results of the improved model with the original linearized model that uses the Boussinesq approximation.

A Technique for Determining the Vertical Distribution of Radiative Equilibrium Temperature Above Jupiter's Clouds

The presence and approximate amounts of ammonia and methane above the clouds of Jupiter have been deduced from spectroscopic observations. Both of these gases have absorption bands in the infrared region of the spectrum and should play an important role in shaping the vertical distribution of radiative equilibrium temperature above the cloud top. The absorption coefficients of these gases are wavelength dependent. Therefore, to compute the radiative equilibrium temperature distribution, we would like to develop a non-grey radiative transfer model applicable to the Jupiter atmosphere. Such a model should be more realistic than the Eddington approximation, which has recently been applied to Jupiter's upper atmosphere by Gross and Rasool [32].

We can divide the infrared region into a finite number of spectral intervals, in each of which the absorption coefficient can be considered constant. For each spectral interval, we will have a different opacity, as follows:

$$\begin{aligned} \tau(z) &= k_1 \int_o^z \rho dz \\ \tau_2(z) &= k_2 \int_o^z \rho dz \\ \tau_n(z) &= k_n \int_o^z \rho dz \end{aligned} \tag{100}$$

where τ is opacity, z is height, k is the absorption coefficient, and ρ is density of absorbing gas. We can relate the opacities of all spectral intervals to a reference opacity, for example, to the opacity of the first spectral interval by the formula

$$\tau_n(z) = \frac{k_n}{k_1} \tau(z) = w_n \tau(z)$$

where w_n is the ratio of the absorption coefficient in the n^{th} spectral interval to the absorption coefficient in the reference spectral interval. The net flux of radiation at the opacity level τ at height z can then be written as

$$F(\tau) = F_1(\tau) + F_2(w_2\tau) + \ldots . F_n(w_n\tau) . \tag{101}$$

The condition for radiative equilibrium requires that

$$\frac{dF(\tau)}{d\tau} = 0 \tag{102}$$

which can be written as

$$\frac{d}{d\tau} \left[F_1(\tau) + F_2(w_2\tau) + \ldots . F_n(w_n\tau)\right] = 0 \quad . \tag{103}$$

The expressions for the net fluxes of radiation at the level τ for the various spectral regions can be written as

$$F_1(\tau) = 2B_1(o)\, E_3(\tau) + 2 \int_o^{\tau} B_1(t)\, E_2(\tau - t)\, dt - 2 \int_{\tau}^{\tau_g} B_1(t)\, E_2(t - \tau)\, dt$$

$$F_2(w_2\tau) = 2B_2(o)\, E_3(w_2\tau) + 2 \int_o^{w_2\tau} B_2(t)\, E_2(w_2\tau - t)\, dt$$

$$- 2 \int_{w_2\tau}^{w_2\tau_g} B_2(t)\, E_2(t - w_2\tau)\, dt \tag{104}$$

$$F_n(w_n\tau) = 2B_n(o)\, E_3(w_n\tau) + 2 \int_o^{w_n\tau} B_n(t)\, E_2(w_n\tau - t)\, dt$$

$$- 2 \int_{w_n\tau}^{w_n\tau_g} B_n(t)\, E_2(t - w_n\tau)\, dt$$

where $B_1(o)$, $B_2(o)$, and $B_n(o)$ are the blackbody fluxes radiated by the cloud top in the 1st, 2nd, and n^{th} spectral region; the E's are exponential integrals, and τ_g is the opacity of the entire atmosphere above the cloud top in the reference spectral interval. After applying the radiative equilibrium condition (103) and simplifying, one can obtain the following expression

$$B_1(\tau) + w_2 B_2(w_2\tau) + \ldots w_n B_n(w_n\tau) =$$

$$+ \frac{1}{2}\left[B_1(o)\ E_2(\tau) + B_2(o)\ w_2 E_2(w_2\tau) + \ldots B_n w_n E_2(w_n\tau)\right]$$

$$+ \frac{1}{2}\int_o^{\tau_g}\left[B_1(t)\ E_1(|\tau-t|) + B_2(t)\ w_2^2\ E_1(w_2|\tau-t|)\right.$$

$$\left. + \ldots\ B_n(t)\ w_n^2\ E_1(w_n|\tau-t|)\right] dt \quad . \qquad (105)$$

At a particular evel, τ, in the atmosphere, the blackbody fluxes in each spectral interv . depend solely on the temperature at that level and can be determined from Planck's law. Thus, if one divides the atmosphere into m levels, one can write an equation similar to Equation (105) for each level. There would be (m +1) unknowns — the temperature at the cloud top and the temperatures at each of the m levels above the cloud top. By imposing the condition that the outgoing infrared radiation must balance the incoming solar radiation at the top of the atmosphere, we can obtain an additional equation that makes it possible to solve for the unknown cloud top temperature and the m unknown atmospheric temperatures. The equation of balance at the top of the atmosphere can be written as

$$2\left[B_1(o)\ E_3(\tau_g) + B_2(o)\ E_3(w_2\tau_g) + \ldots\ B_n(o)\ E_3(w_n\tau_g)\right]$$

$$+2\int_o^{\tau_g}\left[B_1(t)\ E_2(\tau_g-t) + B_2(t)\ E_2(w_2|\tau_g-t|) + \ldots B_n(t)\ E_2(w_n|\tau_g-t|)\right] dt$$

$$= \sigma\ T_e^4$$

where T_e is the effective temperature of the incoming solar radiation and σ is the Stefan-Boltzmann constant. Given T_e and the variation of absorption coefficient with wavelength, it is possible to determine, from the numerical analogues of Equations (105) and (106), the radiative equilibrium temperature distribution from the cloud top to the top of Jupiter's atmosphere.

Survey of the General Circulation of the Jovian Atmosphere

General Remarks. - Jupiter holds the place of eminence among the nine planets of the solar system both in terms of mass and volume. For Jupiter is heavier and occupies more space than all of the other planets together. This giant planet is similar to Venus in that a dense cloudy atmosphere prevents visual or photographic observation of the planet's "surface"; however, telescopic observations of Jupiter reveal a wealth of markings and bands in its atmosphere, quite a contrast to the rather featureless atmosphere of Venus. Because its distance from the sun is five times that of the earth, Jupiter remains always in full phase. Moreover, Jupiter can be observed during the nightime hours as well as the sunrise and sunset positions since it is an outer planet. Owing to its large orbit, this planet has a sidereal period of 11.9 years, a meteorological year considerably longer than that of the earth.

Table 5 shows values of pertinent meteorological parameters for the planet Jupiter. The numbers in parentheses are the magnitude of Jupiter's parameters relative to those for the earth. For example, the equatorial diameter of Jupiter is 11.2 times the earth's diameter.

Jupiter lends itself to several modes of observation from the earth, including visual, photographic, spectroscopic, and radio techniques. In the study of the general circulation of the Jovian atmosphere, we are limited primarily to visual and photographic observations to give us data on aspects of atmospheric circulation.

Observations.

Telescopic view of Jupiter's disc and its nomenclature. - Before we describe the detailed observational features of Jupiter and their relation to the planet's general circulation, let us review the quasi-permanent characteristics of Jupiter's disc as seen through a telescope and their respective nomenclature.

Figure 15 is a diagram of the telescopic view of Jupiter's disc as seen by an earth observer. South is at the top of the diagram and north is at the bottom. It is noticed that the dark strips are called belts, and the light strips are called zones. In the middle of the equatorial zone, there is a thin gray line, the equatorial band. The relative positions of these belts and zones are clearly shown in Figure 15.

Four quasi-permanent belts are located near the equator. Beginning with the most northerly, they are the North Temperate Belt, the North Equatorial Belt, the South Equatorial Belt and the South Temperate Belt. There are two components in the South Equatorial Belt, namely the north component South Equatorial Belt and the south component South Equatorial Belt. The number of belts visible between polar regions and the N. N. Temperate Belt or S. S. Temperate Belt is variable with time.

TABLE 5

METEOROLOGICAL PARAMETERS FOR JUPITER

Parameter	Value
Diameter	
Equatorial	142,700 km (11.2)
Polar	133,200 km (10.4)
Mass	1.9×10^{30} g (318.4)
Density	1.34 g/cm^3 (0.24)
Surface gravity	2.60×10^3 cm/sec^2 (2.65)
Rotation period	
System I (Lat. zone $\leq 12^o$)	9^h50^m 30.003^s (0.41)
System II (Lat. zone $> 12^o$)	9^h55^m 40.632^s
Inclination of equator to orbital plane	3.07^o (.133)
Mean distance from sun	7.78×10^8 km (5.20)
Siderial period of revolution (Jupiter's meteorological year)	11.86 years
Coriolis parameter at pole	3.5×10^{-4} sec^{-1} (2.39)
Albedo	44% (1.26)

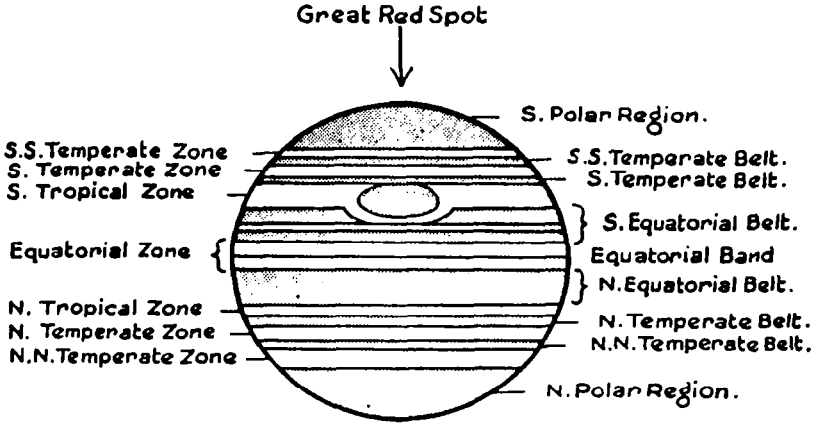

Figure 15. Diagram illustrating the nomenclature used in this report [33].

An outstanding feature os Jupiter's surface is the Great Red Spot located in the S. Tropical Zone. The 'bay' around this oval object in the S. Equatorial Belt is known as the Red Spot Hollow.

These observed features of Jupiter's disc are manifestations of the general circulation of the Jovian atmosphere. Our discussion of the circulation problem below uses the terminology and nomenclature presented in this section.

Zonal and meridional motions of the atmosphere. - Large-scale circulations are evident from the movement of surface markings. Bright or dark spots are a common feature of Jupiter's surface, having lifetimes from several days to a few months. These spots show a zonal movement from west to east as evidenced by their observed time periods of rotation. It is believed that the drift of spots is a direct result of zonal wind currents in the belts and zones.

Observations show that the periods of spots are shorter in the bright equatorial zone and longer at higher latitudes. The region of transition from short to long rotation periods occurs in the dark equatorial belts. Hess [34] has studied the distribution of spot periods on Jupiter with latitude. A summary of his results is shown in Figure 16 where the heavy crosses indicate average periods for the latitude bands and the light circles indicate occasional periods. The line connecting the crosses and circles indicates the hypothetical current distribution with latitude. As indicated in Figure 15, hatched areas represent dark belts and clear areas are light zones. The shorter period implies that the current has higher speed and the longer period implies a lower speed.

Shapiro [35] has made a more thorough study of spot velocities. He found that the average magnitudes of zonal and meridional velocities are 15.1 and 7.5 mph, respectively, and that the mean spot speed is 19.3 mph. An uncertainty of 4 mph exists in these velocities. In the latitudinal region between 12^{o}N and 12^{o}S (System I) the period of rotation is about 9 hours 50.54 minutes in the areas poleward of these latitudes (System II) the period is 9 hours 55.72 minutes. It follows that the zonal velocity of System I is about 100 m sec^{-1} faster than System II. Therefore, a System I spot, having the same relative velocity as a System II spot has a velocity 100 m sec^{-1} faster than the System II spot.

Statistical results in Shapiro's study indicate a tendency for dark spots to move poleward and bright spots to move equatorward. Based on these movements he constructed the 'synoptic charts' shown in Figures 17 and 18. The area between the two dashed lines is System I, and the hatched area is the Great Red Spot. In Figure 17, there appears to be a cyclonic flow in the equatorial side of the Red Spot and an anticyclonic eddy on the lee side. In Figure 19, there appears a subtropical high pressure belt at about 6^{o} to 7^{o}S and a zone of westerlies at 15^{o}N. Based on his analysis, Shapiro believes that spots tend to concentrate in narrow latitudinal zones of 13^{o} to 17^{o} in the Northern Hemisphere and 8^{o} to 17^{o} in the Southern Hemisphere, and that

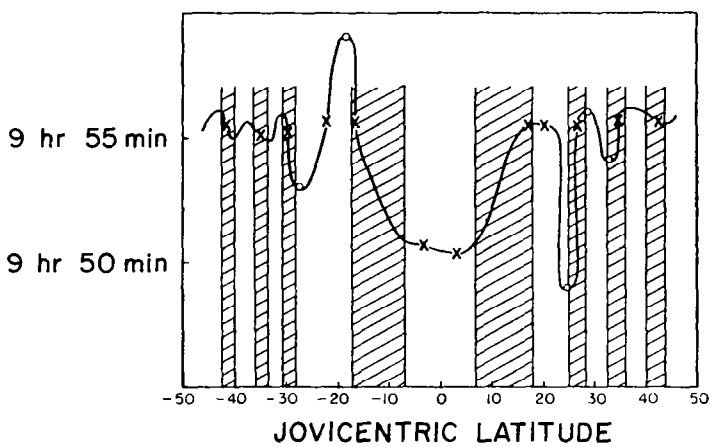

Figure 16. Distribution of spot periods on Jupiter with latitude [34].

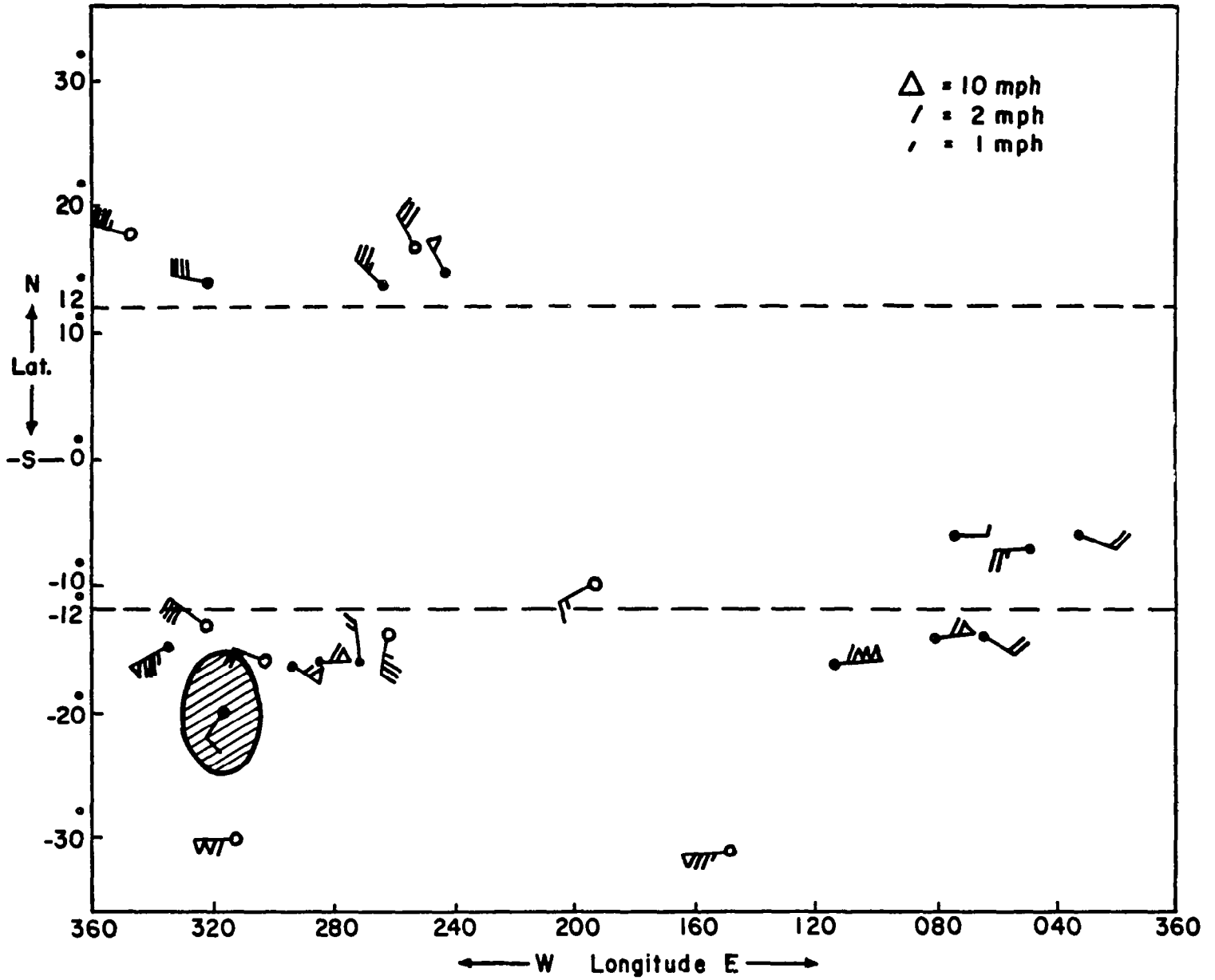

Figure 17. Synoptic spot velocities [35].

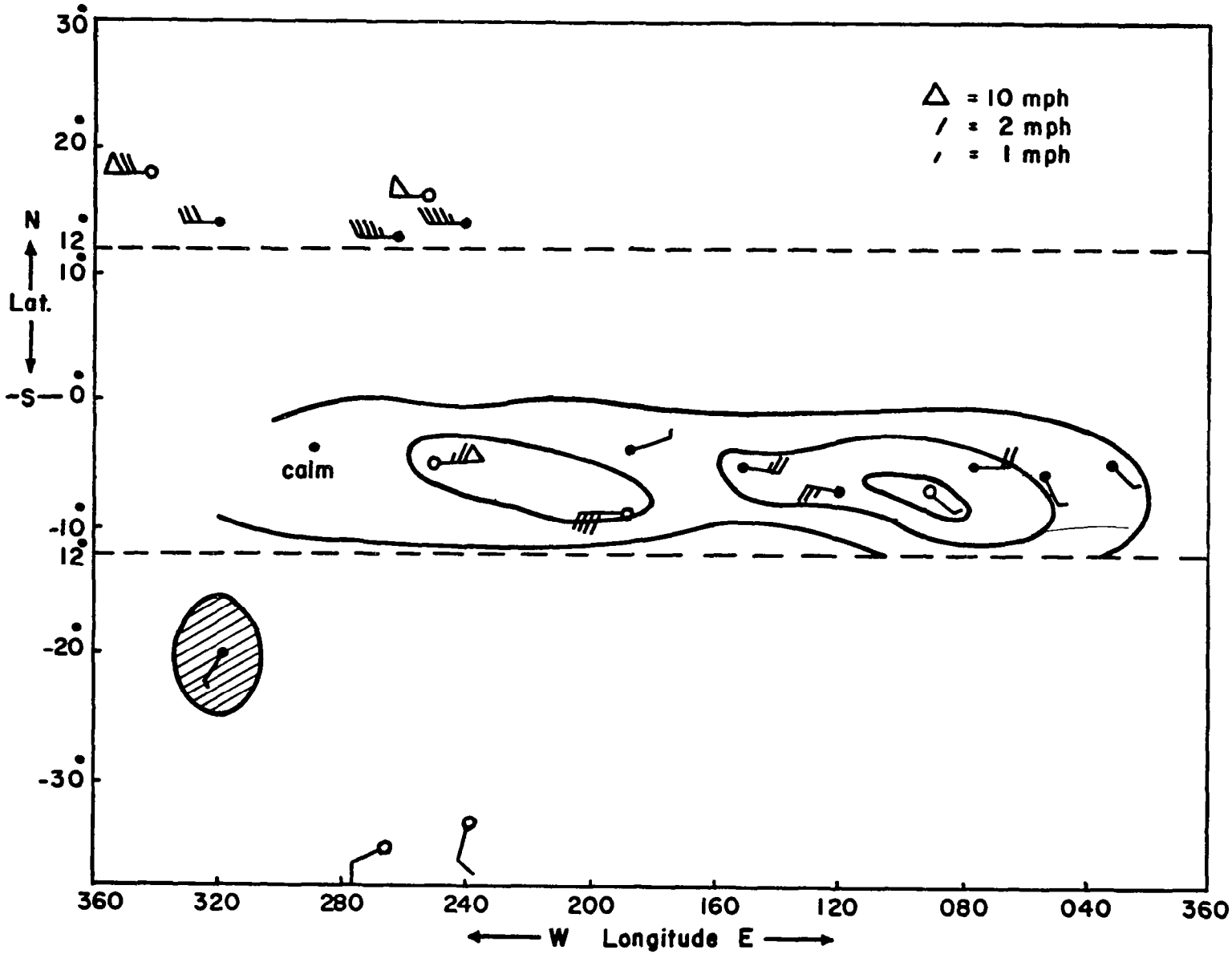

Figure 18. Mean spot velocities for the months of October and November 1928 [35].

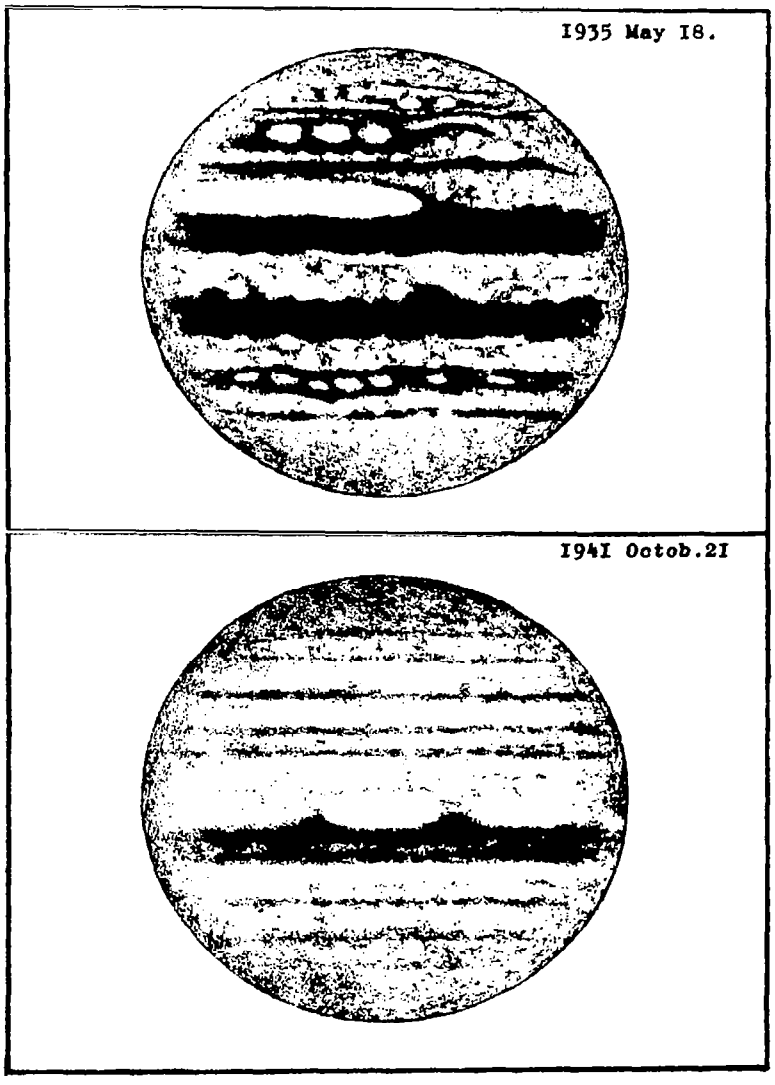

Figure 19. The varying amount of brilliant and dark matter on the planet is criterion of the intensity of atmospheric activity [36]. (a) Maximum activity. (b) Minimum activity.

more spots are found in the Southern Hemisphere than in the Northern Hemisphere. The latter fact is probably due to the existence of the Great Red Spot in the Southern Hemisphere.

Based on the analysis by Hess in Figure 16, it is noticed that the dark belts are regions of cyclonic shear and that bright zones are regions of anticyclonic shear. Similar to the results obtained by Shapiro, Hess [34] indicate that some spots actually show meridional movement as they move zonally and describe an anticyclonic orbit in the Southern Hemisphere of Jupiter. Wave-like patterns often form at boundaries between belts and zones. Rifts often appear in the belts which may persist for months. All of these phenomena are believed to be associated with instabilities in the zonal currents.

Focas [36] pointed out that the prominent character of the activity on Jupiter is the appearance of brilliant and dark matter, and that the apparent amount of brilliant and dark matter gives evidence of the intensity of the atmospheric activity (See Figure 19). Based on the details of the appearance of the brilliant matter in the belts, Focas believes that this process denotes ascending motion in the belts. Narrow strips of a spiral aspect are usually found in association with brilliant spots, suggesting motions around vortices. This particular phenomenon is more pronounced in equatorial and adjacent areas, and less pronounced at higher latitudes. For the last 100 years, spot activity seems to be stronger in the Southern Hemisphere on Jupiter. Also, the activity has a periodic cycle of 20 to 22 years.

Biennial. Biennial oscillation of equatorial wind from the recent decameter wavelength observations of Jupiter, Carr, et al. [37] found that the period of the repeating intensity maximum of radio bursts is 9 hours, 55 minutes, 29.37 seconds. If these bursts issued from a source fixed with respect to the surface, then this period indicates that the rotation period of Jupiter and the relative wind velocity in the troposphere is westerly at 105 m sec^{-1} over the equator and easterly at 4 m sec^{-1} at latitude 20 degrees. From studies of spectrogram inclinations of both Fraunhofer and ammonia lines, Spinrad [38] obtained easterly zonal winds of roughly 3.9 km sec^{-1} to 6.7 km sec^{-1} in the stratosphere over the equator. This supersonic stratospheric zonal wind and strong vertical shear are astonishing. Based on the observational data by Spinrad and Trafton [39], Owen and Staley [40] found that the zonal wind in the Jovian stratosphere shows a 26-month oscillation while the zonal wind in the troposphere remains unchanged as shown in Table 6.

TABLE 6

ZONAL WINDS IN THE JOVIAN STRATOSPHERE DERIVED FROM INCLINATIONS OF AMMONIA ABSORPTION LINES [40]

Date	Slit position across Jovian disc	Inclination of ammonia lines (per cent of Fraunhofer)	Zonal wind in stratosphere (km sec^{-1})	Mean zonal wind in troposphere appropriate to indicated latitude (km sec^{-1})
27 March 1934	Equatorial	23	-6.7	+0.1
3 March 1954	45°N	42	-1.4	-0.003
1 August 1961	Equatorial	34	-3.9	+0.1
23 August 1962	Equatorial	50	+0.1	+0.1
23 August 1962	60°N	50	-0.002	-0.002

This 26-month oscillation is also found above the equator in the terrestrial atmosphere [41]. Figure 20 shows the time cross-section of the vertical profile of the equatorial zonal wind between February 1954 and October 1960 near Canton Island.

Owen and Staley predicted in April 1963 based on the data presented in Table 6, that the deviation of zonal flow from the west should be apparent in the fall of 1963 when the planet Jupiter would be in a favorable position for observations. The suggested observation was made at the Tokyo Astronomical Observatory, Japan, between August and November 1963 and the data were analyzed by Nishida and Jujaku [42]. Although the result is marginal, the anomaly was detected by the Japanese group. More observations are needed for the same period from other observations around the world so that the 26-month oscillation theory can be verified.

The Great Red Spot and related features in the general circulation. - In addition to the outstanding Jovian phenomenon of the equatorial "jet stream" (System I), which has not been observed in other planets, another mystery of the Jovian atmosphere is the Great Red Spot. It has an oval shape with zonal and meridional dimensions of about 40,000 and 13,000 km respectively. The Spot, in general, has a brick red color.

The Spot has been observed since 1664, varying somewhat in zonal speed or longitudinal position and showing slight motion in latitude [43]. The rotation period of the Spot was 9 hours 55 minutes 59 seconds in 1664 to 1666, and 9 hours 55 minutes 54 seconds in 1666 to 1672. The rotation periods varied irregularly between 9 hours 55 minutes 31 seconds and 9 hours 55 minutes 41.5 seconds. During the last hundred years the period has varied between 9 hours 55 minutes 31 seconds and 9 hours 55 minutes 44 seconds [44]. The maximum longitudinal

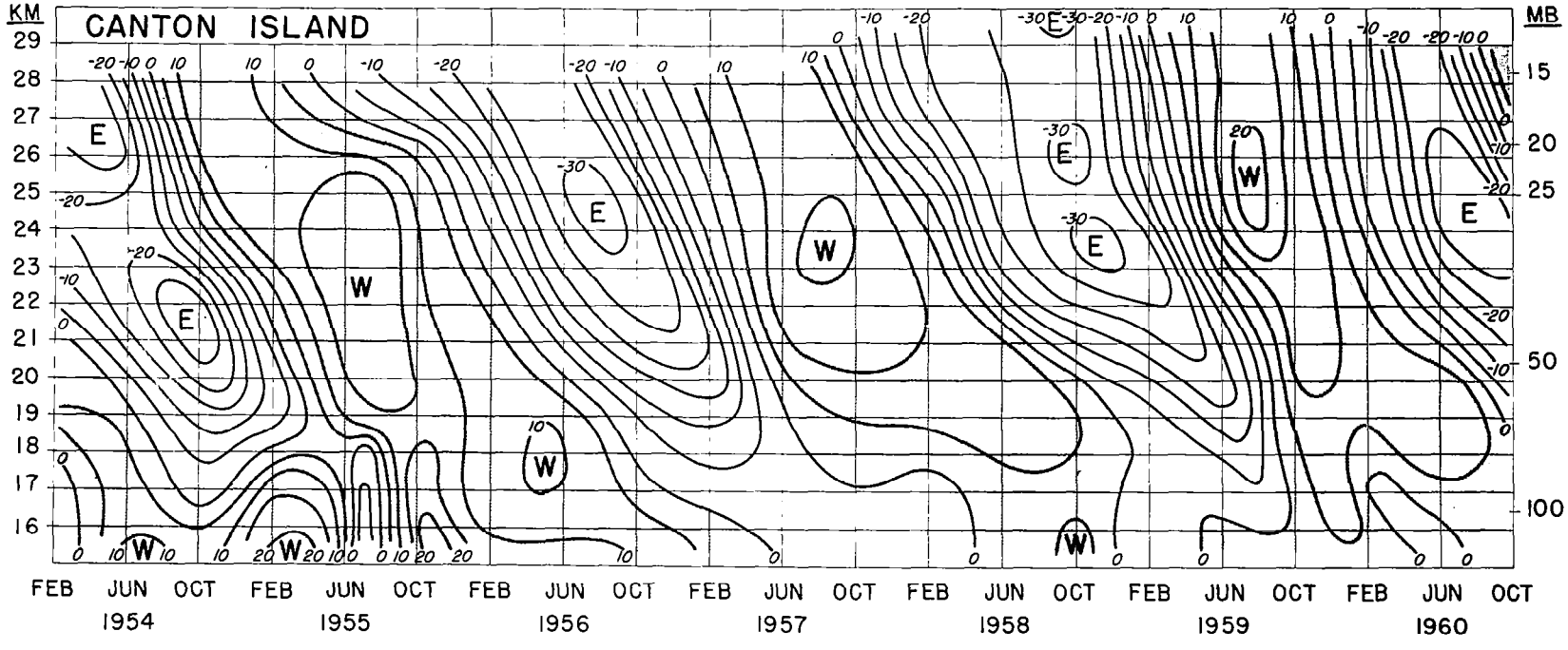

Figure 20. The time cross section of the vertical profile of the equator zonal wind (16-29 km) on earth between February 1954 and October 1960 near Canton Island.

variation of the center of the Spot was reported as being only 1.5 degrees during 1908 to 1930.

Short lived spots in the S. Tropical Zone sweep around the Great Red Spot through the "Red Spot Hollow" with speeds ten times greater than their normal zonal velocities.

Recently Peek [44] made a statistical study of the correlation between the varying rotation period of the Great Red Spot and North Equatorial Current. He found a correlation coefficient of 0.69 based on 30 apparitions between 1891 and 1932-33. However, a negative correlation coefficient of -0.45 was obtained for the 20 apparitions between 1930-31 and 1952-53. A similar reversal of the correlation sign between the darkness and acceleration of the Spot after 1938 was also found. The question of whether the standard method of correlation as such furnishes a suitable approach to the understanding of Jovian phenomena remains to be answered.

Summary of observations. - Let us attempt to summarize the important observational features of the Jovian circulation as follows:

(1) The zonal circulation at low latitudes (System I) is approximately 100 m sec^{-1} faster than the circulation at higher latitudes (System II).

(2) A biennial oscillation of the equatorial wind similar to that in the earth's stratosphere may occur in the Jovian equatorial upper atmosphere.

(3) Three semi-permanent light zones and dark belts are found in both the northern and southern hemispheres. A variable number of belts is observed at polar regions. These phenomena are presumably related to circulation characteristics; the exact relationships are unknown.

(4) The Great Red Spot shows a relatively large motion in longitude but very slight motion in latitude. The Red Spot Hollow is situated on the north side of the Spot and in the S. Equatorial Belt. The existence of the Great Red Spot and the Red Spot Hollow is unique among the planets.

(5) Bright and dark spots have zonal velocities of about 15 mph relative to their own systems. The meridional velocities are about 7.5 mph. The spots are the manifestations of Jovian circulation activity. It is suspected that the formation of the spots is associated with vertical motion in vortices.

Theoretical Studies On the Vertical Extent and Various Phenomena Concerning the General Circulation of the Jovian Atmosphere

The indications of the circulation of the Jovian atmosphere as observed from the earth suggest many interesting and outstanding problems. A few preliminary theoretical studies on the explanation of these observations are outlined in the following sections. Most of the studies are based upon meteorological principles and theories of fluid dynamics. Although these studies have not produced satisfactory answers and verified results, they throw new light on the difficult problem of the general circulation of a remote planet.

The vertical extent of the Jovian atmosphere. - The following method, suggested by Lorenz [45], can be used to determine the vertical extent of the Jovian atmosphere. Based on the fact that System I is faster than System II, one assumes that the total torque exerted on the core by the atmosphere must be zero and, further, that the winds just above a shallow frictional layer next to the core are equal to those at the visible surface. From the balance of torque, one can estimate that the period of the core is about 9 hours 54 minutes 0 seconds and that the speed of the top of the frictional layer is about 35 m sec^{-1}. This value seems rather large.

The solar energy per unit area received by Jupiter is only about 1/27 as much as the earth. With this small incoming energy, the near velocity of circulation can never reach 35 m sec^{-1}. The only possibility is that there is a strong wind at the upper visible surface and a very weak wind at the top of the friction layer. Since System I rotates faster than System II, the geopotential surface in System I is 2.2 km higher at the equator and 49 km lower at the pole than that in System II, based on the geostrophic wind equation. Assuming that the mean temperature contrast at the boundary between System I and System II is about two percent of the temperature at the equator, from the hydrostatic equation or thermal wind equation, Lorenz estimates that the depth of the atmosphere below the visible surface is about 110 km. This result is considered the best theoretical estimate of the height of the visible surface.

Equatorial Acceleration and Meridional Movement of Bright and Dark Spots.- Concerning the equatorial acceleration, Shapiro [35] made an analogy to the jet stream in the earth's atmosphere, considering that the equatorial acceleration consists of two jets at low latitudes in each hemisphere with strong horizontal meridional mixing over the equator. Based upon the dishpan work done by Fultz and Long [46] a jet stream developes at low latitudes for small temperature contrast and rapid rotation. If the planet's rotation is slowed down, the jet stream displaces poleward. Shapiro made a further analogy by relating the spots to migratory cyclones and anticyclones based on the fact that these activities are concentrated on the poleward side of the strong zonal current — jet stream. Such a concentration follows from Kuo's [47] theory of the general circulation of the earth's atmosphere. In Kuo's theory, the effect of the vorticity distribution in the northern hemisphere is such as to exert a horizontal force to drive cyclonic vortices toward regions of higher absolute vorticity — to the north of the jet stream — and anticyclonic vortices toward regions of lower absolute vorticity — to the south of the jet stream. On studying the movement of the dark and bright spots, Shapiro found that dark spots tend to move poleward and bright spots tend to move equatorial similar to movements of cyclones and anticyclones near the terrestrial jet stream. Therefore, he speculates that the dark and bright spots are directly associated with the cyclonic and anticyclonic vortices, respectively, in the Jovian atmosphere. If these spots are well above the tropopause level, the vertical motion will be in a downward direction above a surface cyclone and in an upward direction directly above a surface anticyclone. Since evaporation will take place in downward motion above cyclones,

the spots above surface cyclones will exhibit a relatively dark color. As noted, the observations also indicate that dark spots tend to move poleward, which is also in agreement with the theory that they are upper level manifestations of surface cyclones. The process is just the opposite for spots that move equatorward, these spots are bright and are probably upper level manifestations of surface anticyclones.

Another suggestion concerning the relative westerly momentum in the Jovian atmosphere near the equator is due to Kuiper[48]. He suggested that this westerly momentum might be generated by the collapse of a fossil gaseous ring which is a remnant of the disk that surrounded the planet at the time of planetary formation. However, this collapse ring mechanism becomes questionable in the light of the recent work by Owen and Staley [40] which indicates that huge momentum fluctuations are found at higher layers. Details have been discussed in the section on Survey of the General Circulation of the Jovian Atmosphere.

Biennial Oscillations of the Equatorial Upper Atmosphere Wind. - The reason for the 26-month oscillation of the equatorial upper atmosphere wind is not yet known. However, the solar ultraviolet radiation, annual heating cycle, tidal motion, and the very complicated interactions among the photochemistry of ozone and radiative transfer appropriate to the stratosphere mesosphere, and hydrodynamic stability may be closely related to this quasi-biennial oscillation in the terrestrial atmosphere [41,49,50]. The cause of the 26-month oscillation in the atmosphere of earth and Jupiter maybe similar. In particular, the effects of the UV absorption of methylamine and hydrozine in the spectral region (1000 - 2500Å) and non-effective radiation in the far IR region of methane and ammo ia existing in the Jovian stratosphere might cause strong heating in the stratosphere, which in turn may lead to this 26-month oscillation phenomenon [51].

Great Red Spot and Red Spot Hollow.- The Great Red Spot has been a center of speculation since the fifteenth century. It has been theorized that the Red Spot is a large object with depth comparable to its transverse dimensions, floating either in a liquid or in an "ocean" of highly compressed gases. This hypothesis was investigated theoretically by Sagan [52]. He concluded that this hypothesis is generally unsatisfactory, unless a particular favorable solid state phase transition, which is doubtful at the present time, is operating. Besides, the very slight latitudinal motion of the Great Red Spot does not find a natural explanation in terms of a floating object.

Other speculations and hypotheses based on hydrodynamic theory of rotating fluids have been proposed. If a cylindrical obstacle is moved slowly across the bottom of a rotating tank and the fluid inside has a solid rotation, then dye released well above and in front of the obstacle divides sharply. No horizontal mixing takes place across the vertical imaginary circumscribing cylinder. Dye released in front of the cylinder flows around it as if a solid obstacle had extended throughout the fluid. This is the so-called Taylor column. The theory that explains this phenomenon is due to Taylor and Proudman. The theory states that all steady, slow motions (i.e., Rossby number less than 1) in a rotating inviscid fluid are necessarily two-dimensional.

Based on the experiment by Taylor [53] and the Taylor-Proudman theorem of rotating fluids, Hide [43 & 54] has tried to explain some aspects related to the Spot. The vertical dimension of the obstacle or topographical feature does not have to be enormous to create a Taylor column. As long as the Rossby number near the Spot is much less than 1, a small vertical dimension may satisfy the criterion for forming a Taylor column. Therefore, Hide believes that a topographic feature on the 'mantle' of Jupiter is responsible for the formation of the Great Red Spot.

The Red Spot Hollow also supports the 'topographic feature' theory. The characteristic asymmetry of the Red Spot Hollow accompanied by short-lived spot activity only on the north side of the Great Red Spot and relatively laminar flow on the south side of the Spot, resemble fluid dynamic experiments in the laboratory. Experiments similar to those performed by Taylor are being conducted at Wood's Hole Oceanography Institute. In these experiments, a thread of ink flows with moderate turbulence around — rather than over — a block in a counterclockwise direction relative to the fluid. The creation of moderate turbulence may be similar to the spot activity near the Red Spot Hollow.

Although some properties of the Great Red Spot may be explained by a Taylor column, a proof that a Taylor column does exist is still needed. More work should be performed on the reality of the basic conditions that are necessary to form a Taylor column.

Formation of belts and zones. - There have been no formal theories concerning the formation of belts and zones in the Jovian atmosphere. Stone [55] proposes that the formation of these zonal patterns may be due to a kind of rotational symmetrical instability of large-scale zonal flow in the atmosphere of Jupiter. However, his assumptions are based on a model using the Boussinesq approximation and a constant Coriolis parameter with latitude. The validity of these assumptions for the Jovian atmosphere is questionable.

Summary. - Here we want to summarize the results of theories concerning various aspects of the dynamics and general circulation of Jovian atmosphere. They must be considered as tentative results and remain to be verified by direct observations.

(1) The vertical height of the Jovian atmosphere based on Lorenz's model is about 110 km.

(2) The equatorial acceleration in the Jovian atmosphere consists of two persistent lower latitude jet streams — one in each hemisphere — similar to those of earth, with strong mixing across the equator.

(3) In analogy with the terrestrial atmosphere, the dark spots, which are probably associated with surface cyclones, move poleward across the jet stream and the bright spots, which are probably associated with surface anticyclones, move equatorward.

(4) As in the earth's stratosphere, biennial oscillations of wind apparently occur in the Jovian equatorial stratosphere. This biennial oscillation may be caused by strong heating in the stratosphere.

(5) The Great Red Spot may be a manifestation of a Taylor column caused by a topographic feature on the 'mantle.'

(6) The Red Spot Hollow is believed to be a natural consequence of the existence of the Great Red Spot with an asymmetrical flow pattern near the Spot.

(7) Belts and zones may be due to a kind of symmetrical instability of large scale zonal flow.

Suggestions for Future Research

The explanation of the physical processes causing observed circulation features of the Jovian atmosphere presents us with challenging problems for theoretical research. Future accurate observations will not only provide useful data about the Jovian atmospheric circulation, but will also provide a guide for theoretical work that will further our understanding of the logical Jovian general circulation. Although some of the theories concerning the dynamics of the Jovian atmosphere presented above, shed light on our understanding of individual phenomena, the validity of the assumptions in various models needs thorough investigation. The following examples are typical areas of research.

(1) A comparison should be made of the height of the cloud surface (110 km) with calculated vertical temperature profiles of the troposphere and stratosphere.

(2) The reason for the persistence of jet streams at latitudes below 12^{o} in both hemispheres in Shapiro's explanation of the formation of the equatorial jet stream, needs further work.

(3) Spots arrayed in a series along the axes of the belts, resembling the Von Karman vortex street, and the hydrodynamic conditions explaining the turbulent features in the belts are worthwhile studies.

(4) Taylor column theory for a thick compressible atmosphere should be developed.

(5) Zonal instability theory for the formation of zones and belts is needed for a compressible atmosphere and for a variable Coriolis parameter.

(6) Preferred wave numbers of the large-scale circulation should be determined and compared with actual observations.

CONCLUSIONS AND RECOMMENDATIONS

Meteorology of Mars

Our studies of circulation processes in the Martian atmosphere attempt to synthesize available observations with appropriate meteorological theory. Standard formulae to describe circulation features and frontal phenomena on earth have been adapted for the planet Mars. It should be borne in mind that the following results and conclusions depend on the representativeness of the observations and the magnitudes of assumed values:

(1) There is good evidence that frontal phenomena occur on Mars at low latitudes.

(2) The annual general circulation on Mars appears to be in the wave regime and in geostrophic balance.

(3) The mean zonal wind velocity is 23 to 30 m/sec for a surface pressure of 25 mb and 13 to 16 m/sec for a surface pressure of 85 mb. The corresponding meridional velocities are 1.5 m/sec and 0.6 m/sec, respectively.

(4) Based on a 3 mb depression for a convective vortex model storm, the maximum surface winds may reach speeds of 140 m/sec.

(5) Based upon theoretical estimates of the vertical velocity profile together with analogy with the earth's atmosphere, the Martian troposphere extends to about 20 km.

It is recommended that studies of circulation processes in the Martian atmosphere be continued in an attempt to develop improved estimates based upon more sophisticated theoretical models. Studies designed to estimate the dominant wavelengths of the large scale circulation on Mars from stability theory should be performed. Attempts should be made to develop simple numerical models of the Martian general circulation. In numerical models, it is possible to include the variation of Coriolis force with latitude and non-linear effects. The results of such studies should lead to improved information on mean velocities, circulation patterns, and energy exchange.

Phenomena and atmospheric parameters of importance to the design of systems for manned and unmanned exploration of the planet should be investigated. For example, dust storms appear to be the only "storm" activity that might be of concern to the design of landing missions. Since dust storms also occur on earth, it is suggested that available information on earthly dust storm activity be collected and analyzed so that such weather phenomena can be better understood. Also, improved estimates of maximum surface winds are required for the design of Martian landers. Attempts should be made to obtain such improved estimates.

Meteorology of Venus

From our studies of radiative equilibrium temperatures of the surface and atmosphere of Venus, and circulation processes in the Venusian atmosphere, we arrive at the following conclusions:

(1) With a complete cloud cover, the high observed surface temperatures on Venus can be maintained through a greenhouse mechanism, even with rather modest atmospheric infrared opacities, if the effective infrared emissivity of the cloud layer is about 0.99.

(2) It is tentatively concluded on the basis of an analysis of the results from several circulation models that the mean wind velocity in the Venusian atmosphere is about 2 to 8 m/sec.

(3) It is suggested that the occasionally reported radial spoke system of clouds, centered at the subsolar point, is caused by vertical shear flow in a thermally unstable atmosphere.

It is recommended that a simple combined convective-radiative equilibrium model be applied to Venus for the purpose of obtaining more realistic estimates of the vertical temperature structure. As improved estimates of the amounts of carbon dioxide, water vapor, and other possible absorbing constituents in the entire Venusian atmosphere become available, studies should be made of the absorption of solar radiation by the atmosphere. Improved estimates of surface temperature distribution should be obtained from analysis of available microwave observations; such estimates can be used to study the global circulation of the Venusian atmosphere.

Meteorology of Jupiter

A theoretical model for determining the radiative equilibrium distribution of temperature in the non-grey atmosphere above the Jovian cloud layer has been derived. Calculations with this model should be performed to obtain improved estimates of the vertical temperature profile above the Jovian clouds.

Based upon our general survey of available observational and theoretical information on circulation phenomena in the Jovian atmosphere, we suggest that the following lines of approach might be fruitful ones for increasing knowledge of atmospheric circulations on Jupiter:

(1) critical examination of previous simplifying assumptions in studies of Jovian circulation phenomena, and (2) application of stability theory to the problem of the formation of the belts and zones in the Jovian atmosphere.

LIST OF TECHNICAL REPORTS AND PAPERS PUBLISHED UNDER THE CONTRACT

A number of scientific publications has resulted from the NASA support of our research in planetary meteorology. Listed below are contract technical reports and papers published in the scientific journals.

Contract Technical Reports:

Ohring, G., W. Tang, and G. DeSanto, 1962: Theoretical estimates of the average surface temperatures on Mars. Technical Report No. 1, Contract NASw-286, GCA Technical Report 62-3-N, 23 pp.

Ohring, G., 1962: A theoretical estimate of the average vertical distribution of temperature in the Martian atmosphere. Technical Report No. 2, Contract NASw-286, GCA Technical Report 62-7-N, 15 pp.

Ohring, G., and O. Coté, 1963: The meteorology of Mars and Venus. Annual Technical Report, Contract NASw-286, GCA Technical Report 63-6-N, 82 pp.

Ohring, G., and J. Mariano, 1963: The effect of cloudiness on a greenhouse model of the Venus atmosphere. Contract NASw-704, GCA Technical Report 63-17-N, 28 pp.

Craig, R., 1963: Tides in the atmospheres of earth and Mars. Contract NASw-704, GCA Technical Report 63-26-N, 45 pp.

Ohring, G., E. M. Brooks, and J. Mariano, 1964: The meteorology of Mars and Venus. Final Report, Contract NASw-704, GCA Technical Report 64-4-N, 104 pp.

Tang, W., 1965: Some aspects of the atmospheric circulation on Mars. Contract NASw-975, GCA Technical Report 65-4-N, 43 pp.

Papers Published in Scientific Journals:

Ohring, G., W. Tang, and G. DeSanto, 1962: Theoretical estimates of the average surface temperature on Mars. Journal of the Atmospheric Sciences, 19, 444-449.

Ohring, G., 1962: Theoretical estimates of the average surface and atmospheric temperature on Mars. Memoires de la Societe Royale des Sciences de Liege, 24, 425-447.

Ohring, G., 1963: A theoretical estimate of the average vertical distribution of temperature in the Martian atmosphere. Icarus, 1, 328-333.

Ohring, G., and J. Mariano, 1964: The effect of cloudiness on a greenhouse model of the Venus atmosphere. Journal of Geophysical Research, 69, 165-175.

Ohring, G., and J. Mariano, 1964: Changes in the amount of cloudiness and the average surface temperature of the earth. Journal of the Atmospheric Sciences, 21, 448-450.

Tang, W., 1965: Some aspects of the atmospheric circulation on Mars. Submitted to Journal of Atmospheric Sciences.

REFERENCES

1. LaSeur, N. E. and Jordan, C. L., "A Typical Situation of Typhoon Season," Dept. of Meteor., University of Chicago (1952).

2. Kuiper, G. P., "Visual Observations of Mars, 1956," Ap. J. 125, 307-317 (1957).

3. deVaucouleurs, G., Physics of the Planet Mars, Faber and Faber, Ltd., London, p. 365 (1954).

4. Mintz, Y., "The General Circulation of Planetary Atmospheres, The Atmosphere of Mars and Venus, National Academy of Sciences, National Research Council, Publication 944, pp. 107-146 (1961).

5. Haurwitz, B., "Thermally Driven Circulation," Beitr. Phys. Atm. 35, 145-159 (1962).

6. Ohring, G., Brooks, E. M. and Mariano, J., "The Meteorology of Mars and Venus," Final Report, Contract No. NASw-704, Geophysics Corporation of America, Technical Report No. 64-4-N (1964).

7. Ryan, J. A., "Notes on the Martian Yellow Clouds," J. Geophys. Res. 69, 3759-3770 (1964).

8. Gifford, F., "A Study of Martian Yellow Clouds that Display Movement," Monthly Weather Review 92, 435-440 (1964).

9. Roberts, J. A., "Radio Emission from the Planets," Planetary and Space Sci. 11, 221-260 (1963).

10. Barath, F. T., Barrett, A. H., Copeland, J., Jones, D. E. and Lilley, A. E., "Mariner II: Preliminary Reports on Measurements of Venus — Microwave Radiometers," Science 139, 908-909 (1963).

11. Sagan, C., "The Radiation Balance of Venus," Jet Propulsion Lab. Technical Report, pp. 32-34 (1960).

12. London, J., "A Study of the Atmospheric Heat Balance," Final Report, Contract No. AF19(122)-165, N.Y.U., (ASTIA AD-248155)(1957).

13. Ohring, G. and Mariano, J., "Study of the Average Vertical Distribution of Temperature in the Martian Atmosphere," Final Report, Contract No. NAS9-3423, GCA Technical Report 65-3-N (1965).

14. Arking, A., "Non-Grey Planetary Atmospheres," Proceedings of the Eleventh International Astrophysical Symposium, The Physics of the Planets, University of Liege, Belgium, pp. 180-189 (1962).

15. deVaucouleurs, G., "Geometric and Photometric Parameters of the Terrestrial Planets," ICARMS 3, 187-235 (1964).

16. Ohring, G., Tang, W. and DeSanto, G., "Theoretical Estimates of the Average Surface Temperature on Mars," J. Atmos. Sci. 19, 444-449 (1962).

17. Jastrow, R and Rasool, S. I., "Radiative Transfer in the Atmospheres of Venus and Mars," Space Research III, North Holland Publishing Co., Amsterdam, pp. 1036-1041 (1963).

18. Ohring, G. and Mariano, J., "The Effect of Cloudiness on a Greenhouse Model of the Venus Atmosphere," J. Geophys. Res. 69, 165-175 (1964).

19. Bottema, M., Plummer, W., Strong, J. and Zander, R., "Composition of the Clouds of Venus," Astroph. J. 140, 1640-1641 (1964).

20. Plass, G. N. and Stull, V. R., "Carbon Dioxide Absorption for Path Lengths Applicable to the Atmosphere of Venus," J. Geophys. Res. 68, 1355-1364 (1963).

21. Kuhn, P., "Infrared Flux Soundings and Calculations through an Atmosphere with Clouds," Abstract, Bull. Am. Met. Soc. 45, 707 (1965).

22. Sagan, C. and Kellogg, W. W., "The Terrestrial Planets," Annual Review of Astronomy and Astrophysics 1, 235-266 (1963).

23. Sinton, W. M., "Infrared Observations of Venus," Proc. of Eleventh International Astrophys. Symp., The Physics of the Planets, University of Liege, Belgium, 300-310 (1962).

24. Barath, F. T., "Symposium on Radar and Radiometric Observations of Venus During the 1962 Conjunction," Astronomical J. 69, 1-2 (1964).

25. Kaplan, L. D., "A Preliminary Model of the Venus Atmosphere," Jet Propulsion Lab. Technical Report 32-379, C.I.T (1962).

26. Mintz, Y., "The Energy Budget and Atmospheric Circulation on a Synchronously Rotating Planet," Memorandum RM-3243-JPL, The Rand Corporation, Santa Monica, California (1962).

27. Chandrasekhar, S., Hydrodynamic and Hydromagnetic Stability, Oxford University Press, London (1961).

28. Drake, F. D., "Microwave Observations of Venus, 1962-1963," Astronomical J. 69, 62-64 (1964).

29. Mintz, Y., "Temperature and Circulation of the Venus Atmosphere," Planet. Space Sci. 5, 141-152 (1961).

30. Tang, W., Brooks, E. M., and Watson, B. F., "Theoretical and observational Studies of Vortex Cloud Patterns," GCA Technical Report No. 64-2-G, Contract No. Cwb-10626 (1964).

31. Kuo, H. L., "Perturbation of Plane Couette Flow in Stratified Fluid and Origin of Cloud Streets," Phy. Fluid 6, 195-211 (1963).

32. Gross, S. H. and Rasool, S. I., "The Upper Atmosphere of Jupiter," ICARUS 3, 311-322 (1964).

33. Peek, B. M., The Planet Jupiter, Faber and Faber, London, p. 283 (1958).

34. Hess, S. L., "The Atmosphere of the Other Planets," Compendium of Meteorology, Am. Met. Soc., Boston, p. 1334 (1951).

35. Shapiro, R., "On the Nature of Jovian Spots as Indicated by Their Distribution and Velocities in 1928," In Contributions to the Study of Planetary Atmosphere Circulation, Edited by R. M. White, Geophys. Res. paper No. 24 (Nov. 1953).

36. Focas, J. F., "Preliminary Results Concerning the Atmosphere Activity of Jupiter and Saturn," In Physics of Planets, Proceedings of the Eleventh International Astrophysical Symposium, Liege, Belgium, July 9-12, p. 604 (1962).

37. Carr, T. D., Smith A. G., Bollhagen, H., Six, N. F. Jr., and Chatterton, N. E., "Recent Decameter Wavelength Observations of Jupiter, Saturn and Venus," Ap. J. 134, 105-125 (1961).

38. Spinrad, H., "The Anomalous Inclination of the Jovian Ammonia Lines," Ap. J. 136, 311 (1962).

39. Spinrad, H. and Trafton, C., "High Dispersion Spectra of the Outer Planets - I, Jupiter in the Visual and Red," Icarns 2, 19-28 (1963).

40. Owen, T. C. and Staley, D. O., "A Possible Jovian Analogy to the Terrestrial Equatorial Stratospheric Wind Reversal," J. Atmos. Sci. 20, 347-350 (1963).

41. Reed, R. J., "The Present Status of the 26-Month Oscillation," Paper presented in the 45th Annual Meeting on Jan. 25-28, 1965 in New York, N. Y.

42. Nishida, M. and Jujaku, J., "The Stratospheric Rotation of Jupiter in November 1963," J. Atmos. Sci. 21, 568-569 (1964).

43. Hide, R., "On the Hydrodynamics of Jupiter's Atmosphere," In Physics of Planets, Proceedings of the Eleventh International Astrophysical Symposium, Liege, Belgium, July 9-12, 1962, p. 604.

44. Peek, B. M., "Correlation Between the Varying Rotation Periods of Jupiter's Great Red Spot and North Equatorial Current," Monthly Notice of the Royal Astronomical Soc. 128, 509-512 (1964).

45. Lorenz, E. N., "The Vertical Extent of Jupiter's Atmosphere," In Contribution to the Study of Planetary Atmosphere Circulation, Edited by R. M. White, Geophysical Res. paper No. 24, GRD, AFCRC (Nov. 1953).

46. Long, R. R., "Research on Experimental Hydrodynamics in Relation to Large-Scale Meteorological Phenomena," Progress Report No. 5, Contract No. AF19(122)-160, AFCRL, Bedford, Mass. (1951).

47. Kuo, H. L., "The Motion of Atmospheric Vortices and the General Circulation," J. Meteor. 7, 247-258 (1950).

48. Kuiper, G. P., "The Formation of the Planet, Part I," Roy. Astron. Soc. Can. J. 50, 57-68 (1956).

49. Reed, R. J., "A Tentative Model of the 26-Month Oscillation in Tropical Latitude," Quart. J. Roy. Meteor. Soc. 90, 441-466 (1964).

50. Lindzen, R., "Interactions of Photochemistry and Radiative Transfer with the Hydrodynamics of the Stratosphere-Mesosphere," Paper presented in the 45th Annual Meeting on Jan. 25-28, 1965 in New York, N. Y.

51. Cadle, R. D., "The Photochemistry of the Upper Atmosphere of Jupiter," J. Atmos. Sci. 19, 281-285 (1962).

52. Sagan, C., "On the Nature of the Jovian Red Spot," In Physics of Planets, Proceedings of the Eleventh International Astrophysical Symposium, Liege, Belgium, July 9-12, 1962.

53. Taylor, G. I., "Experiments on the Motion of Solid Bodies in Rotating Fluids," Proc. Roy. Soc. (London), A104, 213-218 (1923).

54. Hide, R., "Origin of Jupiter's Great Red Spot," Nature 190, 895-896 (1961)

55. Stone, P., "On Symmetrical Instabilities of Zonal Currents," Presented at Geophysical Fluid Dynamics Seminar on April 2, 1965 at M.I.T., Boston, Mass (1965).